Clearance of protein aggregates during cell division

Shoukang Du[1,2,3], Yuhan Wang[1,2], Bowen Chen[2], Shuangshuang Xie[2], Kuan Yoow Chan[2,3], David C. Hay[4], Ting Gang Chew[1,2,3,5,#]

Affiliations

[1]Department of Cardiology of the Second Affiliated Hospital, Zhejiang University School of Medicine, Zhejiang University, Hangzhou 310058, China

[2]The Zhejiang University-University of Edinburgh Institute, Zhejiang University School of Medicine, Zhejiang University, Haining 314400, China

[3]College of Medicine and Veterinary Medicine, The University of Edinburgh, Edinburgh, EH4 2XR, UK

[4]Centre for Regenerative Medicine, Institute for Regeneration and Repair, University of Edinburgh, 5 Little France Drive, Edinburgh EH16 4UU, UK

[5]National Key Laboratory of Biobased Transportation Fuel Technology, Zhejiang University, Hangzhou 310027, China

#Correspondending author: Ting Gang Chew (tinggchew@intl.zju.edu.cn)

Abstract

Protein aggregates are spatially organized and regulated in cells to prevent deleterious effects of proteostatic stress. Misfolding of proteins in the ER result in aggregate formation, but how the aggregates are processed especially during cell division is not well understood. Here, we induced proteostatic stress and protein aggregation using a proteostasis reporter, which is prone to misfolding and aggregation in the ER. Unexpectedly, we detected solid-like protein aggregates deposited mainly in the nucleus and surrounded by the ER membrane. The membrane-bound aggregates were then cleared as cells progressed through mitosis and cytokinesis. Aggregate clearance was depended on Hsp70 family chaperones in the ER, particularly BiP, and proteasomal activity. The clearance culminates at mitotic exit and required cyclin-dependent kinase 1 (Cdk1) inactivation but was independent of the anaphase-promoting complex (APC/C). Thus, dividing cells have the capacity to clear protein aggregates to maintain proteostasis in the newly divided cells, which could have implications for human disease development and aging.

Introduction

Nascent polypeptides fold into three-dimensional structures to perform their biological functions (Hipp et al., 2019). Misfolded proteins tend to have their hydrophobic residues exposed and result in aggregation of proteins (Hartl et al., 2011). Intramolecular beta-sheets in some proteins are also structural elements prone for protein aggregation (Tyedmers et al., 2010). Protein misfolding and aggregation not only disrupt the native function of the protein but also could interfere other proteins' functions by co-aggregation (Olzscha et al., 2011; Woerner et al., 2016). This challenges proteome homeostasis (proteostasis) and causes proteostatic stress in cells, which is a main driver of cellular

45 aging and neurodegenerative disorders (Balch et al., 2008; Labbadia and Morimoto, 2015).

46

47 Cells evolve several protein quality control (PQC) systems to maintain their proteostasis in which
48 components of PQC systems facilitate refolding, degradation, and spatial deposition of misfolded
49 protein aggregates (Jayaraj et al., 2020). Molecular chaperones are key players in the PQC system.
50 They are involved to fold nascent polypeptides, target misfolded proteins for degradation by
51 ubiquitin-proteasome system or autophagy, and promote solubilisation of protein aggregates
52 (Tyedmers et al., 2010). Eukaryotic cells confine misfolded proteins and smaller aggregates into
53 distinct cellular deposition sites, which reduce the reactivity of these harmful species to the proteome
54 (Kaganovich et al., 2008). These deposition sites include aggresomes or aggresome-like induced
55 structures locating near centrosomes, INQ (intranuclear quality control compartment) residing in the
56 nucleus, cytosolic CytoQ, and the perivacuolar IPOD (insoluble protein deposit) (Kaganovich et al.,
57 2008). Confinement of protein aggregates in a deposition site facilitates retention of aggregates in
58 short-lived cells (mother cells) during asymmetric cell division (Aguilaniu et al., 2003; Fuentealba et
59 al., 2008; Rujano et al., 2006; Singhvi and Garriga, 2009; Zhou et al., 2014).

60

61 The endoplasmic reticulum (ER) processes one-third of cellular proteome and possesses stronger
62 ability to maintain aggregation-prone proteins in a non-toxic state than the cytosol owing to its
63 specific molecular chaperone environment (Vincenz-Donnelly et al., 2018). Chaperones in the ER
64 such as HSPA5/BiP regulates the unfolded protein response (UPR), which blocks instant protein
65 synthesis and activates transcription of genes involved in PQC (Preissler and Ron, 2019; Wiseman
66 et al., 2022). In addition, the proteostatic stress in the ER triggers ER-associated degradation (ERAD)

67 and ER-phagy to remove misfolded proteins (Mochida and Nakatogawa, 2022; Olzmann et al., 2013).
68 Despite the high capacity of proteostatic stress response in the ER (Rousseau et al., 2004; Vincenz-
69 Donnelly et al., 2018), excessive misfolded proteins still lead to formation of protein aggregates in
70 the ER (Melo et al., 2022; Miyata et al., 2020). In response to protein aggregation in the ER, BiP
71 functions as a disaggregase to promote solubilization of these aggregates. In cells undergoing
72 asymmetric cell division such as in the budding yeast, the ER diffusion barrier and the ER stress
73 surveillance (ERSU) pathway ensure ER protein aggregates are retained preferentially in the short-
74 lived mother cells during cell division (Clay et al., 2014; Pina and Niwa, 2015). How ER protein
75 aggregates are regulated in dividing cells, especially those that do not undergo asymmetric cell
76 division, is less well studied. We addressed the fate of ER protein aggregates in human cells
77 undergoing cell division symmetrically and identified a clearance mechanism of protein aggregates
78 when cells are exiting mitosis.
79
80 **Results**
81 **Targeting a proteostasis reporter to the ER results in protein aggregate formation in the**
82 **nucleus.**
83 To investigate how cells maintain their proteostasis during cell division, we employed a proteostasis
84 reporter consists of a firefly luciferase mutant prone for protein mis-folding and protein aggregation
85 fused to a green fluorescent protein (FlucDM-eGFP) (Gupta et al., 2011). Next, we targeted the
86 reporter to the ER by fusing a ER-targeting sequence at its N-terminus (ER-FlucDM-eGFP).
87 Interestingly, we found that ER-FlucDM-eGFP assembled into visible protein aggregates in the
88 nucleus when stably expressed in mammary epithelial MCF10A cells in the absence of any

89 perturbation of the proteome stability (Figure 1A). The protein aggregates were below detection limit
90 of our microscopy in first 2 days after lentivirus transduction, but progressively accumulated in cells
91 and stabilized in the population several days after lentivirus transduction. This contrasted with a
92 previous study in which the ER-FlucDM-eGFP was transiently expressed in cells and hence did not
93 allow long term tracking of the protein (Sharma et al., 2018). Luciferase activity measurement
94 showed that ER-FlucDM-eGFP has significantly reduced enzymatic activity and was not functional
95 possibly due to mis-folding and protein aggregation (Figure 1B). Moreover, we observed the
96 colocalization of ER-FlucDM-eGFP aggregates and thioflavin T (ThT), a universal dye to detect
97 amyloid fibril, further supporting these aggregates were misfolded protein aggregates (Figure S1B).
98 Thus, expression of ER-FlucDM-eGFP results in proteostatic stress and allows us to study how
99 protein aggregates are regulated in human cells.
100
101 Formation of protein aggregates in the nucleus by ER-FlucDM-eGFP was not limited to MCF10A
102 cells. The protein aggregates were also detected in the nucleus when ER-FlucDM-eGFP was
103 expressed in other cell lines such as A549, MDA-MB-231 and U2OS cells (Figure 1A and S1A).
104 Similar observations were found when the reporter was fused to the red fluorescent protein mCherry
105 or when a different N-terminal signal peptide sequence was used. In addition, when ER-FlucDM was
106 replaced by ER-HaloDM, which is a modified haloalkane dehalogenase prone to mis-folding and
107 aggregation (Melo et al., 2022), we observed similar protein aggregates in the nucleus (Figures 1C
108 and S1C). However, only very low number of cells formed aggregates in the nucleus when intact
109 GFP was targeted to the ER (Figure S1D). Thus, ER-FlucDM-eGFP formed protein aggregates in
110 the nucleus independent of cell line, fluorescent protein types, specific ER targeting sequence and

111 FlucDM.

112

113 Despite localizing in the nucleus, we found that the protein aggregates were surrounded by the ER
114 membrane as stained by the ER-tracker (Figure 1D). To further confirm this, we sectioned the cells
115 and used electron microscopy to observe the protein aggregates. We found that the aggregates
116 were surrounded by a single layer membrane closed to the inner membrane of the nucleus (Figure
117 1E). Thus, the aggregates are intra-nuclear membranous structure surrounded by the ER membrane.

118

119 **Differential and slow turnover of protein aggregates in cells at interphase and mitosis.**
120 Pathological proteins aggregates such as Z-α1-antitrypsin accumulated in the ER exhibited minimal
121 turnover (Dickens et al., 2016). To test whether ER-FlucDM-eGFP aggregates has a reduced
122 dynamics as well, we performed fluorescence recovery after photobleaching (FRAP) in cells
123 expressing both ER-FlucDM-eGFP and ER-FlucDM-mCherry. The ER-FlucDM-eGFP signal served
124 as a tracker for the location of aggregates and the ER-FlucDM-mCherry was used to probe the
125 aggregate dynamics. We photobleached ER-FlucDM-mCherry with 561 nm laser while ensuring ER-
126 FlucDM-eGFP signal was not affected. In interphase cells, ER-FlucDM-mCherry aggregates
127 intensity barely recovered after 4.5 min post-bleaching, indicating that ER-FlucDM-mCherry
128 aggregates possessed minimal turnover similar to that of in other protein aggregates such as Z-α1-
129 antitrypsin (Figure 2A). Similarly, ER-HaloDM-eGFP aggregates in the nucleus also displayed low
130 recovery after photobleaching (Figure S2A). When ER-FlucDM-mCherry aggregates were
131 photobleached in mitotic cells, the recovery of intensity was also much lesser than the ER-FlucDM-
132 mCherry signal present in the ER network (Figures 2B and 2C). However, ER-FlucDM-mCherry

133 aggregates in mitotic cells showed a higher recovery than that of in interphase cells (Figure 2D;
134 aggregates of interphase cells recovered from 0.131 ± 0.093 to 0.157 ± 0.095; aggregates of mitotic
135 cells recovered from 0.196 ± 0.137 to 0.356 ± 0.151).
136
137 Consistently, the single-cell analysis revealed that in mitotic cells, there was an increase of the
138 recovery intensity of ER-FlucDM-mCherry in late time-point as compared to that of in early time-
139 points after photobleaching. The increased recovery intensity was not observed in ER-FlucDM-
140 mCherry aggregates of interphase cells (Figure S2B). Taken together, ER-FlucDM-mCherry
141 aggregates in the nucleus have low turnover and the aggregate displays increased turnover in mitotic
142 cells.
143
144 **Protein aggregates are cleared during cell division.**
145 Since aggregates displayed some levels of turnover during mitosis (Figures 2B, 2C and 2D), we next
146 investigated the aggregate behaviour throughout cell division. To this end, we labelled cells
147 expressing ER-FlucDM-eGFP with SiR-Tubulin to distinguish cells at various stages based on the
148 microtubule organization. We categorized cells into interphase and prophase, prometaphase,
149 metaphase, anaphase, telophase and early G1 cells based on their microtubule structures (Figure
150 3A). Next, we analyzed the number and area of aggregates in cells of each category. Interestingly,
151 we observed that the number and area of aggregates in telophase and early G1 cells were
152 significantly lower than in interphase cells, suggesting that aggregates are cleared gradually when
153 cells progress through mitosis and cytokinesis (Figure 3B).
154

155 To test whether this was the case, we employed time-lapse imaging to profile aggregates in cells
156 undergoing division. To increase the number of dividing cells during imaging, we synchronized cells
157 at G2/M and released them into mitosis prior to imaging. We observed that upon entry into mitosis,
158 the ER-FlucDM-eGFP aggregates were released from the nucleus during nuclear envelope
159 breakdown and gradually decreased in numbers as cells progress through mitosis and cytokinesis
160 (Figure 3C and Video 1). In majority of early divided G1 cells, there was essentially no detectable
161 aggregates (Figure 3D). Interestingly, the aggregates released from the nucleus during mitosis were
162 still surrounded by the ER membrane as indicated by the ER-tracker (Figures S3A and S3B). The
163 decrease of aggregates appears to happen specifically in dividing cells as the number and area of
164 aggregates remained largely unchanged in interphase cells (Figures 3C and 3D). Furthermore,
165 aggregates formed in cells expressing ER-HaloDM-eGFP decreased in numbers when cells
166 progress through mitosis and cytokinesis (Figure S3C and Video 2), suggesting that the clearance
167 of protein aggregates during cell division was not specific to ER-FlucDM-eGFP.
168
169 **Effects of ER stress inducers on aggregate clearance in mitotic cells**.
170 Expression of ER-FlucDM-eGFP results in proteostatic stress in cells. Consistently, we observed
171 that gene expression for chaperones and co-chaperones in the ER were upregulated in these cells
172 (Figure 4A), indicating cells involved ER proteostasis control during adaptation. We speculated that
173 acute perturbation to ER homeostasis could exacerbate the proteostatic stress in dividing cells
174 expressing ER-FlucDM-eGFP and affect aggregate clearance during mitosis. To test if this was the
175 case, synchronized cells expressing ER-FlucDM-eGFP were released into mitosis in the presence
176 of either DMSO (control) or 1 μM thapsigargin (Thaps), which blocks the ER calcium ion pump and

177 causes ER stress. In cells at prometaphase and metaphase (35 min after release), DMSO and Thaps
178 treatments showed comparable number and area of aggregates in cells (Figures 4B and 4C).
179 However, in cells at the late stage of cell division (65 min after release), there were significantly
180 higher number of aggregates retained in the cytosol of Thaps-treated cells than DMSO (Figures 4B
181 and 4C). Consistently, time-lapse microscopy revealed that ER-FlucDM-eGFP aggregates retained
182 in the cytosol after cytokinesis in Thaps-treated cells, whereas the aggregates were largely cleared
183 in control cells completing cytokinesis (Figures 4D, 4E, S4A and Video 4). Thus, acute treatment of
184 ER stress inducer Thaps in dividing cells prevents clearance of ER-FlucDM-eGFP aggregates.
185
186 A previous study showed that cells with protein aggregates treated for hours with Thaps or
187 Tunicamycin (Tuni), which inhibits protein glycosylation in the ER, promotes aggregate clearance in
188 cells (Melo et al., 2022). To test if prolonged treatment of cells expressing ER-FlucDM-eGFP with
189 Tuni could promote aggregate clearance, we pretreated cells blocked at G2/M with varying
190 concentrations of Tuni for 3 hours and released cells into mitosis. Interestingly, prolonged
191 pretreatment of Tuni prior to mitosis promoted aggregate clearance in dividing cells (Figure S4B).
192 Thus, acute treatment of cells expressing ER-FlucDM-eGFP with ER stress inducers prevents
193 aggregate clearance in dividing cells while prolonged treatment with ER stress inducers promotes
194 aggregate clearance.
195
196 **Hsp70 family protein BiP is required for aggregate clearance during cell division.**
197 Since we observed that the expression of a chaperone Hsp70 (HSPA5/BiP) was upregulated in cells
198 expressing ER-FlucDM-eGFP (Figure 4A) and Hsp70 is involved in elimination of protein aggregates

199 (Melo et al., 2022; Nillegoda et al., 2015), we next tested whether the clearance of ER-FlucDM-eGFP
200 aggregates in dividing cells was mediated by Hsp70 family proteins. To this end, cells entering
201 mitosis were treated with either DMSO (control) or VER-155008 (VER), an inhibitor of HSP70's
202 ATPase activity (Samanta et al., 2021). We found that VER-treated dividing cells fixed after 65
203 minutes released from the G2/M boundary retained high number of ER-FlucDM-eGFP aggregates
204 in the cytosol compared to control treatment (Figures 5A and 5B). Time-lapse microscopy showed
205 that when cells were treated with VER, ER-FlucDM-eGFP aggregates released from the nucleus
206 upon entry into mitosis were not cleared as to the same extent as control cells (Figure 5C and Video
207 5).
208
209 HSPA5/BiP is a major Hsp70 family member in regulating ER proteostasis. We next tested whether
210 inhibition of BiP function could affect clearance of aggregates in dividing cells. Similar to VER
211 treatment, inhibition of BiP's ATPase activity by YUM-70 (Samanta et al., 2021) led to a dose-
212 dependent accumulation of ER-FlucDM-eGFP aggregates in cells (Figures 5D and 5E). Moreover,
213 by using immunofluorescence staining, we found a strong colocalization of BiP and ER-FlucDM-
214 eGFP, consistent with a role of BiP in regulating ER-FlucDM-eGFP aggregates (Figures S5A and
215 S5B). Collectively, our data demonstrated that the clearance of ER-FlucDM-eGFP aggregates was
216 regulated by the HSP70 family proteins, particularly BiP.
217
218 **Aggregate clearance is a mitotic exit event but is independent of the anaphase promoting**
219 **complex (APC/C)**.
220 Protein aggregates are subjected to proteasomal degradation in cells (Tyedmers et al., 2010). To

221 test if aggregate clearance during cell division involves proteasomes, we inhibited the proteasome
222 activity with MG132 in dividing cells expressing ER-FlucDM-eGFP. After treating cells released from
223 the G2/M boundary with low or high concentrations of MG132 for 55 minutes, majority of mitotic cells
224 were arrested at metaphase and accumulated high number of aggregates as compared to control
225 cells treated with DMSO (Figures S6A and S6B). Next, we inhibited the proteasome with MG132 in
226 cells at late anaphase or telophase and examined the aggregates 35 minutes after MG132 treatment
227 (Figures S6C and S6F). In cells completing cytokinesis, there were significantly high number of
228 aggregates in the early divided cells treated with MG132 versus the control (Figures S6D, 6E, S6G
229 and S6H)
230
231 Since protein aggregates are cleared when cells progress through mitosis and cytokinesis, which
232 are the cell cycle stage with low Cyclin B/CDK1 activity, we speculated that inactivation of CDK1
233 activity in MG132-treated and metaphase-arrested cells could lead to clearance of ER-FlucDM-
234 eGFP aggregates in the cytosol. To test if this was the case, we released cells into mitosis in the
235 presence of MG132 for 55 minutes and treated metaphase-arrested cells with RO-3306 to inhibit
236 Cdk1 activity (Figure 6A). Interestingly, ER-FlucDM-eGFP aggregates were cleared in cells treated
237 with RO-3306 while the aggregates were retained in cells treated with DMSO (Figures 6B and S6I).
238 Consistently, live cell imaging demonstrated similar accelerated clearance in Cdk1 inhibited cells
239 (Figures 6C and 6D). Thus, clearance of the aggregates happens when cells exit from mitosis.
240
241 We established that clearance of aggregates during cell division requires proteasomes and CDK
242 inactivation, it is possible that the anaphase promoting complex (APC/C), which is a E3 ubiquitin

243 ligase regulating mitotic exit (Watson et al., 2019), is involved in clearing the aggregates. To test if
244 this was the case, we inhibited APC/C activity using a cocktail of APC/C inhibitors (APC/Ci) consists
245 of Apcin and ProTAME in dividing cells expressing ER-FlucDM-eGFP (Sackton et al., 2014).
246 Interestingly, inhibition of APC/C did not affect aggregate clearance as APC/Ci-treated cells that have
247 arrested at metaphase have comparable number of aggregates as in control DMSO-treated cells
248 (Figures 6E and 6F). When cells at late anaphase or telophase were treated with APC/Ci, the newly
249 divided cells have similar number of aggregates as in control cells (Figures 6G, 6H and 6I). Lastly,
250 we verified the efficacy of APC/C inhibition using cells expressing the APC/C reporter derived from
251 Geminin (Figure S6J). Consistently, APC/Ci treatment has prevented the removal of APC/C reporter
252 in newly divided cells indicating that the APC/C was inhibited by the dosage of APC/Ci used in our
253 experiments (Figure S6K). Taken together, our data showed that clearance of ER-FlucDM-eGFP
254 aggregates happens when cells exit from mitosis, is proteasome dependent but does not involve
255 APC/C.
256

257 **Discussion**

258 We showed that stably expression of ER-FlucDM-eGFP leads to proteostatic stress and formation
259 of protein aggregates in human cells without the use of additional proteostatic stressors. This
260 fluorescent based live-cell imaging reporter enables us to study how protein aggregates are
261 regulated in dividing cells, which are sensitive to genetic or environmental perturbations.
262 Conventional methods that use proteasomal inhibitors to cause proteome imbalance are not ideal to
263 investigate proteostasis in dividing cells given an essential role of protesomes in driving mitotic exit
264 (Ghislain et al., 1993; Glotzer et al., 1991). Additionally, methods such as heat shock also perturb

265 mitotic progression, especially in human cells (Kakihana et al., 2019). By using ER-FlucDM-eGFP
266 that does not perturb cell cycle progression, we reveal an unexpected process of clearing protein
267 aggregates in cells progressing through mitosis and cytokinesis.
268
269 Previous studies showed that the proteome of mitotic cells have higher structural stability and less
270 aggregation prone compared to that of in interphase cells (Becher et al., 2018; Wirth et al., 2013).
271 Post-translational modifications such as phosphorylation of mitotic proteins are suggested to be
272 responsible for the protein stability during cell division (Becher et al., 2018). The aggregate clearance
273 we identified in this study could represent an active mechanism that increases proteome stability in
274 dividing cells. We found that aggregate clearance requires Cdk1 inactivation, which is a hallmark of
275 mitotic exit, however, does not involve APC/C that is important in driving mitotic exit through protein
276 degradation. It is possible that APC/C targets mostly cytosolic proteins whereas ER-FlucDM-eGFP
277 aggregates are confined in a membrane during mitosis. Furthermore, the clearance of protein
278 aggregates coincides with ER reorganization that happens throughout mitosis and cytokinesis, which
279 may contribute to the aggregate clearance (Bergman et al., 2015; Schlaitz et al., 2013).
280
281 Misfolded or damaged proteins form protein aggregates and are spatially organized into specific
282 subcellular sites to sequester them from other cellular processes (Hill et al., 2017). These aggregate
283 deposition sites are localized in the cytosol or in the nucleus to confine misfolded proteins and
284 aggregates for elimination from cells (Kaganovich et al., 2008). Similarly, we identified confinement
285 of ER-FlucDM-eGFP aggregates in the nucleus and are surrounded by a single layer membrane.
286 These intranuclear membranous structures contain ER membranes and BiP, which is a key Hsp70

287 family chaperone in the ER and translocates into the nucleus under stress (Liu et al., 2023). How
288 protein aggregates are targeted and assembled into the intranuclear membranous structure awaits
289 future investigation. Interestingly, upon entry into mitosis, concomitant with the nuclear membrane
290 breakdown, the membranous structure is released from the nucleus and the aggregates are cleared
291 when cells progress though mitosis till early G1 phase of the daughter cells. The confinement and
292 clearance of protein aggregates during cell division presumably protect dividing cells from harmful
293 effects of protein misfolding and aggregation and to ensure reliable inheritance of genetic materials.
294 It has been reported that aggregates are asymmetrically retained in one of the daughter cells that
295 are usually short-lived (Rujano et al., 2006). The aggregate clearance mechanism we report here
296 may provide an additional cellular defense strategy to overcome proteostatic stress and to maintain
297 proteome integrity during cell division.
298
299 Hsp70 chaperones regulate proteostasis by preventing protein aggregation, promoting
300 disaggregation and subjecting solubilized aggregates to degradation or refolding (Rosenzweig et al.,
301 2019). A recent study showed that BiP solubilizes aggregates and drives aggregate clearance in the
302 ER (Melo et al., 2022). Our study of mitotic aggregate clearance in dividing cells further extend the
303 role of BiP in disaggregation. Consistently, we found that Cdk1 inactivation in the presence of the
304 proteasomal inhibitor could still lead to aggregate clearance, suggesting a partial role of the
305 proteosome in clearing aggregates and the disaggregation breaks down the aggregates into smaller
306 and possibly soluble species. Interestingly, Melo et al. showed that aggregate clearance is promoted
307 by treating cells with ER stressors as the treatment triggers UPR, which in turn leads to higher activity
308 of BiP to cope with the ER stress. We observed differential responses of aggregate clearance to ER

309 stressors depending on the duration of the treatments (Figure 4). It is possible that acute treatment
310 of the ER stressor on dividing cells does not provide sufficient time for cells to accumulate abundant
311 amount of BiP given that mitotic cells are not very transcriptionally active (Palozola et al., 2017). Also,
312 degradation of BiP could be accelerated upon the treatment of ER stressors, which in turn
313 undermines the abundance of BiP in disaggregation (Shim et al., 2018). Thus, short term treatment
314 of the ER stressor in cells exacerbates the ER stress and affects aggregate clearance during cell
315 division, whereas longer treatment of the ER stressor promotes aggregate clearance. Mechanistic
316 understanding of aggregate clearance during cell division could offer new insights to understand
317 disaggregation in proteostasis control.
318

319 **Materials and methods**

320 **Cell lines and culture**

321 MCF10A cells were cultured in DMEM F-12 (Sigma) supplemented with 1% Glutamax (Gibco), 5%
322 horse serum (Biological Industries), 20 ng/ml EGF (Gibco), 0.5 mg/ml Hydrocortisone
323 (MedChemExpress), 100 ng/ml Cholera toxin (Sigma), 10 μg/ml Insulin (Biological Industries), and
324 1% Pen/Strep (Biological Industries). U2OS, A549, and HEK293Ta cells were maintained in DMEM
325 (Sigma) with Glutamax (Gibco), 6% fetal bovine serum (Biological Industries), and 1% Pen/Strep
326 (Biological Industries). MDA-MB-231 cells were cultured in DMEM F-12 (Sigma) with 1% Glutamax
327 (Gibco) and 1% Pen/Strep (Biological Industries). All cell cultures were maintained at 37°C with 5%
328 CO_2 in a humidified incubator. Cells expressing ER-FlucDM-eGFP, ER-eGFP, ER-HaloDM-eGFP,
329 ER-FlucWT-eGFP, and ER^{FSHR}-FlucDM-eGFP, ER-FlucDM-mCherry were generated through
330 lentivirus transduction and selected with 5 μg/mL puromycin (Sangon Biotech). MCF10A cells co-

331 expressing ER-FlucDM-eGFP and ER-FlucDM-mCherry for FRAP or co-expressing ER-FlucDM-
332 mCherry and mGreenLantern-hGeminin (degron) were generated by lentivirus transduction and
333 selected by 5 ug/mL puromycin and followed by fluorescence-activated cell sorting (FACS) to enrich
334 double-positive cells.
335
336 **Lentivirus packaging**
337 Lentiviral particles were generated using the 3rd generation lentiviral packaging system. Packaging
338 plasmids pRSV-Rev, pMDLg/pRRE, pMD2.G (kindly provided by Didier Trono) and the transfer
339 plasmid were chemically transfected using GeneTwin transfection reagent (Biomed, TG101) into the
340 HEK293Ta packaging cell line (Genecopoeia, LT008). The cell culture medium was harvested after
341 2 days and filtered through a 0.45 μm filter. The filtrate was concentrated using a 5X precipitation
342 solution (250 g/L PEG 8,000 and 43.83 g/L NaCl in ddH_2O) for overnight, and precipitated by
343 centrifuging at 4000 ×g for 25 min at 4°C. Lentiviral particles were resuspended in phosphate
344 buffered saline (PBS) and added to the culture medium, which were supplemented with 1 μg/mL
345 polybrene (HanBio).
346
347 **Lentivirus expression constructs**
348 Lentiviral transfer plasmids used in this study were listed below: pTGL0563 containing FlucDM-eGFP
349 in which FlucDM was mutated from FlucWT (a gift from Dr. Mikael Bjorklund); pTGL0645 containing
350 ER-FlucDM-eGFP-KDEL; pTGL0673 containing ER-FlucDM-mCherry-KDEL; pTGL0698 containing
351 ER-FlucWT-eGFP-KDEL; pTGL0703 containing ER-HaloDM-eGFP-KDEL in which HaloDM was
352 mutated from HaloWT; pTGL0707 containing ER-HaloWT-eGFP-KDEL; pTGL0733 containing ER -

353 eGFP-KDEL; pTGL0743 containing ER^{FSHR}-FlucDM-eGFP; pTGL0828 containing mGreenLantern-
354 hGeminin (degron).
355
356 **Quantitative real-time PCR (qPCR)**
357 Total RNA was extracted from cells using the FastPure Cell/Tissue Total RNA Isolation Kit V2
358 (Vazyme, RC112-01). Subsequently, the RNA was reversely transcribed into complementary DNA
359 (cDNA) using the HiScript II Q RT SuperMix for qPCR (Vazyme, R223-01). The levels of the cDNAs
360 were quantified using real-time PCR with the ChamQ Universal SYBR qPCR Master Mix (Vazyme,
361 Q711-02). The PCR reaction mix was prepared on a hard-shell PCR plate (Bio-Rad, HSP9655),
362 sealed with Microseal 'B' seals (Bio-Rad, MSB1001), and conducted in the CFX96 Touch Real-Time
363 PCR Detection System (Bio-RAD, C1000). Primers used in the qPCR: GAPDH, 5'
364 CAGGAGGCATTGCTGATGAT 3' and 5' GAAGGCTGGGGCTCATTT 3'; HSPA5, 5'
365 CACAGTGGTGCCTACCAAGA 3' and 5' TGTCTTTTGTCAGGGGTCTTT 3'; Calreticulin, 5'
366 ATAAAGGTTTGCAGACAAGC 3' and 5' CCACAGTCGATGTTCTGCTC 3'; HSP90B1, 5'
367 TCCAGCAGAAAAGAGGCTGA 3' and 5' CAAATTCGGGAAGGGCCTGA 3'; CANX, 5'
368 GCACCTATTCTGGAGGCGAG 3' and 5' ACAGCAACCACTTCCCTTCC 3'; P4HB, 5'
369 TTCAGGAATGGAGACACGGC 3' and 5' TCCACGTCCTTGAAGAAGCC 3'; DNAJB9, 5'
370 GTGGAGGAGCAGCAGTAGTC 3' and 5' CGCTCTGATGCCGATTTTGG 3'. The C_T value for
371 GAPDH was used for normalization to obtain the relative expression level.
372
373 **Luciferase activity test**
374 Each well of 96-well plates (Biosharp, BS-MP-96W for luminescence, BS-MP-96B for fluorescence)

375 was seeded with 10,000 cells in 100 μL of medium. After incubation for 18 hours, 5 μM MG132 was
376 added to the MG132+FlucDM-eGFP group, while other untreated wells remained unchanged.
377 Following an additional 6 hours, cells were washed once with PBS.
378
379 For luminescence detection, cell lysis was achieved by adding 50 μL of Steady-Glo Luciferase Assay
380 System buffer (Promega, E2510) to the wells, followed by a 15-minute incubation at room
381 temperature. Luminescence in each well was then recorded three times over 5 minutes using the
382 Spark® Multimode Microplate Reader (Tecan, 1000 ms exposure). Luminescence intensity in each
383 well was calculated by normalizing these three measurements and subtracting the background signal
384 from empty wells.
385
386 To determine relative specific luciferase activities, the luminescence values were divided by the
387 fluorescence intensity of eGFP. Cells were immediately immersed in PBS after the PBS wash. Within
388 3 minutes, eGFP fluorescence intensity was measured by selecting the GFP channel of the Tecan
389 microplate reader mentioned above. Fluorescence intensity in each well was calculated by
390 subtracting the background signal from empty wells.
391
392 **Mitotic cell preparation**
393 To increase the quantity of dividing cells, cells were first seeded on imaging chambers (ibidi, 80826)
394 and were synchronized to the G2/M boundary by treating cells with 7.5 μm RO-3306 (Selleckchem,
395 S7747) for 16 to 20 hours. Cells were released to enter into mitosis synchronously by washing once
396 with pre-warmed fresh medium.

397

398 **Drug treatments**

399 The following drugs were used in this study: Thapsigargin (Abcam, ab120286), MG132 (CSN Pharm,
400 CSN11436), YUM70 (Aladdin, Y413413), VER-155008 (CSN Pharm, CSN13116), Apcin (Sigma,
401 SML1503), proTAME (Cayman Chemical, 25835).

402

403 **Immunofluorescence staining**

404 For HSPA5/BiP staining, MCF-10A cells expressing ER-FlucDM-eGFP were seeded in 8-well ibidi
405 plates, fixed with 100% methanol for 10 minutes and permeabilized with 0.5% Triton X-100 for 15
406 minutes. The fixed cells were blocked with 5% FBS in PBS for 30 minutes. Subsequently, cells were
407 incubated with the mouse anti-BiP antibody (HuaBio, HA601076) at 1:200 dilution in 1% FBS
408 overnight at 4°C. The secondary antibody used was Donkey Anti-Mouse IgG H&L (Alexa Fluor® 568,
409 ab175472, Abcam) at 1:2000 dilution for one hour. For Tubulin staining, cells were fixed using 4%
410 PFA for 20 minutes and permeabilized with 0.5% Triton X-100 for 15 minutes. After blocking the fixed
411 cells with 5% FBS in PBS for 30 minutes, cells were stained with the mouse anti-α-tubulin
412 monoclonal antibody (Proteintech, 66031-1-IG) at 1:200 dilution. The secondary antibody used was
413 Donkey Anti-Mouse IgG H&L (Alexa Fluor® 568, ab175472, Abcam) at 1:2000 dilution for one hour.
414 To stain DNA, DAPI Staining Solution (Sangon Biotech, E607303, 5 mg/L) was diluted in PBS to 50
415 ng/mL and applied to cells for 10 minutes. After the DAPI solution was removed, fixed cells were
416 washed with PBS twice before imaging.

417

418

419 **Transmission Electron Microscopy (TEM)**

420 To prepare samples for TEM, MCF10A cells expressing ER-FlucDM-eGFP were synchronized to the
421 G2/M boundary by treating cells with RO-3306 for 16 to 20 h and were released into mitosis by
422 removing RO-3306. After 45 min released from the G2/M boundary, cells were trypsinized for 10 min
423 before centrifugation. The cell pellet was fixed by 2.5% paraformaldehyde (in PBS) for 30 min at
424 room temperature before overnight at 4°C. Fixed pellet was further fixed by 1% osmium tetroxide
425 and then 2% uranium acetate. Ethanol and acetone were used to dehydrate samples before
426 embedding them into epoxy resin. Sectioned samples were observed by Tecnai G2 spirit 120kV
427 transmission electron microscopy (Thermo FEI).

428

429 **Live-cell staining**

430 The live-cell staining dyes used are as follow: 100 nM SiR-Tubulin (Cytoskeleton, CY-SC002), 1 μM
431 ER-tracker Red (Beyotime, C1041S) or 10 μM Thioflavin T (ThT) in the medium to label cells for
432 about 30 min in the incubator before imaging. For ThT staining, about ten percent aggregates could
433 be stained by ThT in ER-FlucDM-mCherry cells.

434

435 **Spinning-disk confocal microscopy imaging**

436 The hardware configuration of the spinning-disk confocal microscopy system was as described
437 previously (Wang et al., 2023). Imaging utilized a z-step size of 0.5 μm, with a x-y plane resolution
438 of 183.3 nm/pixel for the 60× lens and 110 nm/pixel for the 100× lens. Fluorophores were excited
439 using laser lines at wavelengths of 405, 488, 561, or 640 nm.

440

For FRAP analysis, images were acquired with 488 nm and 561 nm laser lines through the 100× lens. The procedure involved acquiring three pre-bleach images every 30 seconds, followed by bleaching the mCherry signal using the 561 nm laser. Subsequently, one image was acquired immediately post-bleaching, followed by ten images acquired every 30 seconds. In total, fourteen time-point images were acquired, and the total duration of each FRAP experiment was 6.5 minutes.

Image analysis and processing

Fiji was used to process images. All Z-stack images for quantification were first projected using max-intensity projection (Fiji/image/stacks/Z project). To quantify aggregates, projected images were classified by Trainable Weka Segmentation (Fiji/Plugins/Segmentation/Trainable Weka Segmentation). The segmented images were processed by using the ImageJ Macro commands: run("8-bit"); setOption("BlackBackground", true); run("Convert to Mask"); run("Watershed") before using Analyze Particles (Fiji/Analyze/Analyze Particles). For time-lapse images except images from FRAP, the segmented images were processed by using the ImageJ Macro commands: run("8-bit"); setThreshold(0, 120); run("Make Binary", "method=Default background=Light black"); run("Invert LUT"); run("Watershed", "stack") before using Analyze Particles (Fiji/Analyze/Analyze Particles).

For FRAP analysis of ER-eGFP and ER-HaloDM-eGFP, region-of-interests (ROI) in projected images were manually selected and the average fluorescence intensity of ROIs was measured in Fiji. For FRAP analysis of aggregates in cells co-expressing ER-FlucDM-eGFP and ER-FlucDM-mCherry (both interphase and mitosis), the aggregates were first segmented by Weka Segmentation. The unsegmented images from the mCherry channel were processed by Analyze Particles

463 (Fiji/Analyze/Analyze Particles) based on the corresponding segmented images from the GFP
464 channel. For fluorescence intensity quantification, background in all FRAP experiments were
465 subtracted by one hundreds.
466
467 **Quantification and statistical analysis**
468 Datasets were analysed by Student's t test or Mann-Whitney test. Prism 8 (GraphPad) was usedfor
469 the statistical analysis and data plotting. Statistical details are indicated in the figure legends.
470
471 **Author contributions**
472 S.D conceived the study, designed and performed experiments, and analyzed data. Y.W, B.C, S.X,
473 K.Y.C provided some reagents used in the study. D.H participated in the discussion during project
474 development. T.G.C. conceived the study, designed experiments and supervised the study. D.S and
475 T.G.C prepared the manuscript with inputs from D.H.
476
477 **Acknowledgements**
478 This study was funded by National Natural Science Foundation of China (NSFC) grant (32270770) and
479 NSFC RFIS-II grant (32350610247) given to T.G.C. We thank Xiaoxia Wan and Chenyu Yang in the
480 Center of Cryo-Electron Microscopy (CCEM), Zhejiang University for their technical assistance on
481 Transmission Electron Microscopy. We thank Xuqi Chen, Xukai Gao and Zihan Chu for participating in
482 the early stage of the project. We thank Dr. Mike Shipston for participating in the discussion. We thank all
483 lab members for discussion.
484

485 **Figure legends**

486 **Figure 1. ER-FlucDM-eGFP forms protein aggregates in the nucleus.**

487 (A) Representative images of ER-FlucDM-eGFP expressed in different cell lines.

488 (B) Quantification of the luciferase activity in MCF10A cells expressing different constructs. Unpaired
489 t-test. Data were collected from three independent experiments.

490 (C) Representative images to show MCF10A cells expressing ER-FlucDM-mCherry, ER^{FSHR}-
491 FlucDM-eGFP (signal peptide sequence from the N-terminus of FSHR), ER-HaloDM-eGFP or
492 ER-eGFP.

493 (D) Images of ER-FlucDM-eGFP aggregates surrounded by the ER membrane in a MCF10A cell.

494 (E) TEM images of sectioned MCF10A interphase cells expressing ER-FlucDM-eGFP.

495 Data represent mean + SD. Scale bar, 10 μm (A to D).

496

497 **Figure 2. Differential aggregate dynamics in cells at interphase and mitosis.**

498 (A) Representative images of interphase cells co-expressing ER-FlucDM-eGFP and ER-FlucDM-
499 mCherry before and after photobleaching. Yellow rectangles indicate bleached aggregates.

500 (B) Representative images of mitotic cells co-expressing ER-FlucDM-eGFP and ER-FlucDM-
501 mCherry before and after photobleaching. Yellow circles indicate bleached aggregates.

502 (C) Recovery curves of ER-FlucDM-mCherry intensity after photobleaching. 14 ROIs from the ER of
503 interphase cells, 14 aggregates from mitotic cells, 26 aggregates from interphase cells. Data
504 represent mean + SD.

505 (D) Quantification of the ER-FlucDM-mCherry intensity of bleached aggregates right after bleaching
506 and after 5 min of recovery. 0 min and 5 min refer to the time points in (C). Paired t-test (two-

507 tailed).

508 Data were collected from four independent experiments. Scale bar, 10 μm.

509

510 **Figure 3. Aggregates are cleared during cell division.**

511 (A) Representative images of dividing ER-FlucDM-eGFP cells at different cell cycle phases. Grey

512 scale bar: telophase and early G1 cells; black scale bar: interphase and prophase, prometaphase,

513 metaphase, anaphase. Scale bar, 10 μm.

514 (B) Quantification of ER-FlucDM-eGFP aggregates from dividing cells. Count and area are individual

515 cell data. Each grey ring represents aggregates from one cell. Interphase and prophase, 91 cells;

516 prometaphase, 45 cells; metaphase, 60 cells; anaphase, 20 cells; telophase and early G1, 73

517 cells. From three independent experiments. Unpaired two side Mann-Whitney U-test. Data

518 represent mean ± SD

519 (C) Representative time-lapse images of cells expressing ER-FlucDM-eGFP released from the G2/M

520 boundary. NEB (nuclear envelop breakdown) is set to be t = 0 min. Scale bar, 10 μm.

521 (D) Quantification of aggregate number and area of dividing cells expressing ER-FlucDM-eGFP. Left

522 panel: data of individual cells. Right panel: mean values + SD of single-cell data (left panel). Time

523 point of NEB in each cell was set to 0 min. Aggregate count and total area of each cell at each

524 time point is normalized to its own value at t = 0 min. Aggregate count data are from 61 interphase

525 and 73 dividing cells of four independent experiments. Aggregate area of each cell is calculated

526 from 32 interphase and 34 dividing cells of two independent experiments.

527

528

529 **Figure 4. Effects of ER stressors on aggregate clearance.**

530 (A) Relative gene expression levels of chaperones and co-chaperones in cells expressing ER-
531 FlucDM-eGFP. Four independent experiments.

532 (B) Images of cells treated with DMSO or 1 μM Thaps and fixed at 35 min or 65 min after released
533 from the G2/M boundary.

534 (C) Quantification of cells treated with DMSO or 1 μM Thaps and fixed at 35 min or 65 min after
535 released from the G2/M boundary. 35 min_DMSO, 207 cells; 35 min_Thaps, 173 cells;
536 65min_DMSO, 244 cells; 65 min_Thaps, 209 cells. Unpaired two side Mann-Whitney U-test. The
537 solid black line in violin plot indicates median of data in the column. Gray dotted lines are quartiles.
538 Each light pink circle indicates measurements of individual cells.

539 (D) Representative time-lapse images of cells expressing ER-FlucDM-eGFP treated with DMSO or
540 1 μM Thaps after released from the G2/M boundary.

541 (E) Quantification of cells expressing ER-FlucDM-eGFP treated with DMSO or 1 μM Thaps. Time
542 point of NEB in each cell was set to 0 min. Aggregates count and total area of each cell is
543 normalized to its own value at t = 0 min. Black dotted lines are 90 min since NEB. DMSO, 89
544 cells; Thaps, 65 cells.

545 Scale bar, 10 μm. Three (C and E) or four (A) independent experiments.

546

547 **Figure 5. Inhibition of HSP70 and BiP prevents aggregate clearance.**

548 (A) Representative images of cells expressing ER-FlucDM-eGFP treated with DMSO or 50 μM VER
549 and fixed at 65 min after released from the G2/M boundary.

550 (B) Quantification of cells expressing ER-FlucDM-eGFP treated with DMSO or 50 μM VER and fixed

551 at 65 min after released from the G2/M boundary. DMSO, 357 cells; VER, 465 cells.

552 (C) Time-lapse images of dividing cells expressing ER-FlucDM-eGFP treated with DMSO or 50 μM

553 VER.

554 (D) Representative images of cells expressing ER-FlucDM-eGFP treated with DMSO or different

555 concentrations of YUM70.

556 (E) Quantification of cells expressing ER-FlucDM-eGFP treated with DMSO or YUM70 and fixed at

557 65 min after released from the G2/M boundary. DMSO, 310 cells; 5 μM YUM70, 258 cells; 20 μM

558 YUM70, 215 cells; 50 μM YUM70, 209 cells; 100 μM YUM70, 287 cells.

559 Scale bar, 10 μm. Unpaired two side Mann-Whitney U-test. Each solid line in violin plot indicates

560 median of data in the column. Gray dotted lines are quartiles. A, B, D and E are from three

561 independent experiments. C is from two independent experiments

562

563 **Figure 6. Effects of MG132, APCi and RO-3306 (Cdk1i) on aggregate clearance.**

564 (A) Representative images of cells expressing ER-FlucDM-eGFP arrested at mitosis by MG132 and

565 further treated with Cdk1i to induce mitotic exit. Cells were first treated with 25 μM MG132 for 55

566 min and mitotic arrested cells were further treated with 25 μM MG132 plus 10 μM RO-3306 or

567 25 μM MG132 only. Cells were fixed 40 min after the second treatment.

568 (B) Quantification of (A). MG132 only, 442 cells; MG132 + RO-3306, 374 cells.

569 (C) Time-lapse images of cells expressing ER-FlucDM-eGFP arrested at mitosis by MG132 and

570 further treated with RO-3306 to induce mitotic exit. Cells were treated with 25 μM MG132 for 55

571 min, and further treated with 25 μM MG132 plus 10 μM RO-3306 or 25 μM MG132 before imaging.

572 (D) Quantification of (C). Remaining aggregates at 40 min were calculated for their aggregates count

573 or area and compared to that of in 0 min. MG132 only, 125 cells; MG132 + RO-3306, 134 cells.

574 (E) Images of cells expressing ER-FlucDM-eGFP treated with DMSO or APCi (20 μM proTAME and

575 300 μM Apcin) and fixed at 55 min after released from the G2/M boundary.

576 (F) Quantifications of cells expressing ER-FlucDM-eGFP treated with DMSO or APCi (20 μM

577 proTAME and 300 μM Apcin). DMSO, 450 cells; APCi, 549 cells.

578 (G) Images of cells at telophase or cells of newly divided upon treatment of DMSO or APCi for 35 to

579 40 min.

580 (H) Cells at telophase or newly divided cells that have aggregates upon treatment of DMSO or APCi

581 were counted.

582 (I) Aggregates number and area were counted in cells at telophase or in newly divided cells after

583 treated with DMSO or APCi. Only cells with aggregates were included in the quantification.

584 DMSO, 297 cells; APCi, 319 cells.

585 Scale bar, 10 μm. Data are from at least three independent experiments and analysed by unpaired

586 two side Mann-Whitney U-test (B, D, F and I) or paired t-test (H).

587

588

589

590

591

592

593

594

595 **Supplementary figures**

596 **Figure S1. ER-FlucDM-eGFP forms protein aggregates, related to Figure 1**

597 (A) Quantification of ER-FlucDM-eGFP aggregate number (left) and total aggregate area (right) of
598 individual cells in different cell lines. MCF-10A, 516 cells; A549, 395 cells; MDA-MB-231, 369
599 cells; U2OS, 528 cells. Three independent experiments.

600 (B) Colocalization of ER-FlucDM-eGFP and Thioflavin T (ThT), a marker for protein aggregates.

601 (C) Schematic representation of different constructs used in this study.

602 (D) Quantification of aggregate number (left) and total aggregate area (right) in cells expressing ER-
603 eGFP, ER-HaloWT-eGFP, ER-HaloDM-eGFP. ER-eGFP, 612 cells; ER-HaloWT-eGFP, 405 cells;
604 546 ER-HaloDM-eGFP, 546 cells; ER-FlucDM-eGFP, 516 cells. Three independent experiments.

605 Data represent mean + SD. Scale bar, 10 μm.

606

607 **Figure S2. FRAP analysis of protein aggregates, related to Figure 2.**

608 (A) Recovery curve of ER-HaloDM-eGFP before and after photobleaching. Seven interphase cells
609 from three independent experiments. Data represent mean + SD.

610 (B) Recovery curve of individual cell data in ER-FlucDM-eGFP before and after photobleaching. 14
611 ROIs from the ER of interphase cell, 14 aggregates from cells at mitosis, 26 aggregates from
612 cells at interphase. Data were collected from four independent experiments.

613 (C) Recovery curve of ER-eGFP before and after photobleaching. Seven interphase cells from three
614 independent experiments. Data represent mean + SD.

615 (D) Quantification of protein fluorescence intensity of different constructs right after photobleaching
616 and 5 min after recovery. 0 min is the protein intensity right after photobleaching and 5 min is the

617 protein intensity 5 min after recovery from photobleaching. At least three independent
618 experiments. Data represent mean ± SD.
619
620 **Figure S3. Aggregates in dividing cells, related to Figure 3.**
621 (A) Images to show ER-FlucDM-eGFP aggregates of dividing cells were surrounded by the
622 membrane stained by the ER-tracker. Scale bar, 10 μm.
623 (B) TEM images of sectioned MCF-10A mitotic cells expressing ER-FlucDM-eGFP.
624 (C) Time-lapse images of cells expressing ER-HaloDM-eGFP released from the G2/M boundary.
625 NEB (nuclear envelop breakdown) is set to be t = 0 min. Scale bar, 10 μm.
626 (D) Linear regression analysis to show that cell division process is not linearly dependent on
627 aggregates quantity. 74 dividing cells are from four independent experiments.
628
629 **Figure S4. Effect of Thapsigargin or Tunicamycin on aggregates clearance, related to Figure**
630 **4.**
631 (A) Changes of aggregate number and total area as a function of time after cells expressing ER-
632 FlucDM-eGFP were treated with DMSO or 1 μM Thaps.
633 (B) Quantification of aggregate number and total area of cells expressing ER-FlucDM-eGFP treated
634 with DMSO or Tunicamycin (Tuni) during mitosis. DMSO, 542 cells; 200 ng/mL Tuni, 385 cells;
635 2 μg/mL Tuni, 471 cells; 10 μg/mL Tuni, 439 cells. Four independent experiments. Unpaired two
636 side Mann-Whitney U-test. Each solid thick line in violin plot indicates median of data in the
637 column. Gray lines are quartiles.
638

639 **Figure S5. Colocalization of BiP and ER-FlucDM-eGFP, related to Figure 5.**

640 (A) Immunofluorescence staining of BiP and ER-FlucDM-eGFP.

641 (B) Colocalization analysis of BiP and ER-FlucDM-eGFP. R represents Pearson correlation

642 coefficient (r).

643 Scale bar, 10 μm. Three independent experiments.

644

645 **Figure S6. MG132, APCi and RO-3306 treatments on aggregate clearance, related to Figure 6.**

646 (A) Quantification of the aggregate number in cells expressing ER-FlucDM-eGFP treated with DMSO

647 or 25 μM MG132 and fixed at 55 min after released from the G2/M boundary. DMSO, 293 cells;

648 MG132, 350 cells.

649 (B) Quantification of the aggregate number in cells expressing ER-FlucDM-eGFP treated with DMSO

650 or 5 μM MG132 and fixed at 55 min since release. DMSO, 295 cells; MG132, 436 cells.

651 (C) Images of cells at telophase or newly divided cells after treated with DMSO or 25 μM MG132 for

652 35 min.

653 (D) Cells at telophase or newly divided cells that have aggregates upon treatment of 25 μM MG132

654 were counted. DMSO, 455 cells; MG132, 393 cells.

655 (E) Aggregates number and area were counted in cells at telophase or in newly divided cells after

656 treated with DMSO or 25 μM MG132. Only cells with aggregates were included in the

657 quantification. DMSO, 294 cells; MG132, 339 cells.

658 (F) Images of cells at telophase and newly divided cells after treated with DMSO or 5 μM MG132 for

659 35 min.

660 (G) Cells at telophase or newly divided cells that have aggregates upon treatment of DMSO or 5 μM

661 MG132. DMSO, 676 cells; APCi, 646 cells.

662 (H) Aggregates number and area were counted in cells at telophase or in newly divided cells after
663 treated with DMSO or 5 μM MG132. Only cells with aggregates were included in the
664 quantification. DMSO, 227 cells; MG132, 297 cells.

665 (I) Quantification of the aggregate number in cells expressing ER-FlucDM-eGFP treated with 5 μM
666 MG132 or 5 μM MG132 + RO-3306.

667 (J) Images of cells co-expressing ER-FlucDM-mCherry and mGreenLantern-hGeminin (degron).
668 Left panel: cells were treated with DMSO or APC/Ci after 65 min released from the G2/M. Right
669 panel: after 65 min released from the G2/M, cells were treated with DMSO or APC/Ci for 40
670 minutes using live-cell imaging.

671 (K) Quantification of mGreenLantern-hGeminin (degron) intensity of cells treated with DMSO or
672 APC/Ci for 40 min.

673 Scale bar, 10 μm. Data are from at least three independent experiments and analysed by unpaired
674 two side Mann-Whitney U-test (A, B, E, H and I), unpaired t-test (K) and paired t-test (D and G).

675

676 **References**

677 Aguilaniu, H., L. Gustafsson, M. Rigoulet, and T. Nystrom. 2003. Asymmetric inheritance of
678 oxidatively damaged proteins during cytokinesis. *Science*. 299:1751-1753.

679 Balch, W.E., R.I. Morimoto, A. Dillin, and J.W. Kelly. 2008. Adapting proteostasis for disease
680 intervention. *Science*. 319:916-919.

681 Becher, I., A. Andres-Pons, N. Romanov, F. Stein, M. Schramm, F. Baudin, D. Helm, N. Kurzawa, A.
682 Mateus, M.T. Mackmull, A. Typas, C.W. Muller, P. Bork, M. Beck, and M.M. Savitski. 2018.
683 Pervasive Protein Thermal Stability Variation during the Cell Cycle. *Cell*. 173:1495-1507
684 e1418.

685 Bergman, Z.J., J.D. McLaurin, A.S. Eritano, B.M. Johnson, A.Q. Sims, and B. Riggs. 2015. Spatial
686 reorganization of the endoplasmic reticulum during mitosis relies on mitotic kinase cyclin A in
687 the early Drosophila embryo. *PLoS One*. 10:e0117859.

688 Clay, L., F. Caudron, A. Denoth-Lippuner, B. Boettcher, S. Buvelot Frei, E.L. Snapp, and Y. Barral.
689 2014. A sphingolipid-dependent diffusion barrier confines ER stress to the yeast mother cell.

690 *Elife*. 3:e01883.
691 Dickens, J.A., A. Ordonez, J.E. Chambers, A.J. Beckett, V. Patel, E. Malzer, C.S. Dominicus, J.
692 Bradley, A.A. Peden, I.A. Prior, D.A. Lomas, and S.J. Marciniak. 2016. The endoplasmic
693 reticulum remains functionally connected by vesicular transport after its fragmentation in cells
694 expressing Z-alpha1-antitrypsin. *FASEB J*. 30:4083-4097.
695 Fuentealba, L.C., E. Eivers, D. Geissert, V. Taelman, and E.M. De Robertis. 2008. Asymmetric
696 mitosis: Unequal segregation of proteins destined for degradation. *Proc Natl Acad Sci U S A*.
697 105:7732-7737.
698 Ghislain, M., A. Udvardy, and C. Mann. 1993. S. cerevisiae 26S protease mutants arrest cell division
699 in G2/metaphase. *Nature*. 366:358-362.
700 Glotzer, M., A.W. Murray, and M.W. Kirschner. 1991. Cyclin is degraded by the ubiquitin pathway.
701 *Nature*. 349:132-138.
702 Gupta, R., P. Kasturi, A. Bracher, C. Loew, M. Zheng, A. Villella, D. Garza, F.U. Hartl, and S.
703 Raychaudhuri. 2011. Firefly luciferase mutants as sensors of proteome stress. *Nat Methods*.
704 8:879-884.
705 Hartl, F.U., A. Bracher, and M. Hayer-Hartl. 2011. Molecular chaperones in protein folding and
706 proteostasis. *Nature*. 475:324-332.
707 Hill, S.M., S. Hanzen, and T. Nystrom. 2017. Restricted access: spatial sequestration of damaged
708 proteins during stress and aging. *EMBO Rep*. 18:377-391.
709 Hipp, M.S., P. Kasturi, and F.U. Hartl. 2019. The proteostasis network and its decline in ageing. *Nat*
710 *Rev Mol Cell Biol*. 20:421-435.
711 Jayaraj, G.G., M.S. Hipp, and F.U. Hartl. 2020. Functional Modules of the Proteostasis Network.
712 *Cold Spring Harb Perspect Biol*. 12.
713 Kaganovich, D., R. Kopito, and J. Frydman. 2008. Misfolded proteins partition between two distinct
714 quality control compartments. *Nature*. 454:1088-1095.
715 Kakihana, A., Y. Oto, Y. Saito, and Y. Nakayama. 2019. Heat shock-induced mitotic arrest requires
716 heat shock protein 105 for the activation of spindle assembly checkpoint. *FASEB J*. 33:3936-
717 3953.
718 Labbadia, J., and R.I. Morimoto. 2015. The biology of proteostasis in aging and disease. *Annu Rev*
719 *Biochem*. 84:435-464.
720 Liu, Z., G. Liu, D.P. Ha, J. Wang, M. Xiong, and A.S. Lee. 2023. ER chaperone GRP78/BiP
721 translocates to the nucleus under stress and acts as a transcriptional regulator. *Proc Natl*
722 *Acad Sci U S A*. 120:e2303448120.
723 Melo, E.P., T. Konno, I. Farace, M.A. Awadelkareem, L.R. Skov, F. Teodoro, T.P. Sancho, A.W. Paton,
724 J.C. Paton, M. Fares, P.M.R. Paulo, X. Zhang, and E. Avezov. 2022. Stress-induced protein
725 disaggregation in the endoplasmic reticulum catalysed by BiP. *Nat Commun*. 13:2501.
726 Miyata, T., D. Hagiwara, Y. Hodai, T. Miwata, Y. Kawaguchi, J. Kurimoto, H. Ozaki, K. Mitsumoto, H.
727 Takagi, H. Suga, T. Kobayashi, M. Sugiyama, T. Onoue, Y. Ito, S. Iwama, R. Banno, M.
728 Matsumoto, N. Kawakami, N. Ohno, H. Sakamoto, and H. Arima. 2020. Degradation of
729 Mutant Protein Aggregates within the Endoplasmic Reticulum of Vasopressin Neurons.
730 *iScience*. 23:101648.
731 Mochida, K., and H. Nakatogawa. 2022. ER-phagy: selective autophagy of the endoplasmic
732 reticulum. *EMBO Rep*. 23:e55192.
733 Nillegoda, N.B., J. Kirstein, A. Szlachcic, M. Berynskyy, A. Stank, F. Stengel, K. Arnsburg, X. Gao, A.
734 Scior, R. Aebersold, D.L. Guilbride, R.C. Wade, R.I. Morimoto, M.P. Mayer, and B. Bukau.

735 2015. Crucial HSP70 co-chaperone complex unlocks metazoan protein disaggregation.
736 *Nature*. 524:247-251.
737 Olzmann, J.A., R.R. Kopito, and J.C. Christianson. 2013. The mammalian endoplasmic reticulum-
738 associated degradation system. *Cold Spring Harb Perspect Biol*. 5.
739 Olzscha, H., S.M. Schermann, A.C. Woerner, S. Pinkert, M.H. Hecht, G.G. Tartaglia, M. Vendruscolo,
740 M. Hayer-Hartl, F.U. Hartl, and R.M. Vabulas. 2011. Amyloid-like aggregates sequester
741 numerous metastable proteins with essential cellular functions. *Cell*. 144:67-78.
742 Palozola, K.C., G. Donahue, H. Liu, G.R. Grant, J.S. Becker, A. Cote, H. Yu, A. Raj, and K.S. Zaret.
743 2017. Mitotic transcription and waves of gene reactivation during mitotic exit. *Science*.
744 358:119-122.
745 Pina, F.J., and M. Niwa. 2015. The ER Stress Surveillance (ERSU) pathway regulates daughter cell
746 ER protein aggregate inheritance. *Elife*. 4.
747 Preissler, S., and D. Ron. 2019. Early Events in the Endoplasmic Reticulum Unfolded Protein
748 Response. *Cold Spring Harb Perspect Biol*. 11.
749 Rosenzweig, R., N.B. Nillegoda, M.P. Mayer, and B. Bukau. 2019. The Hsp70 chaperone network.
750 *Nat Rev Mol Cell Biol*. 20:665-680.
751 Rousseau, E., B. Dehay, L. Ben-Haiem, Y. Trottier, M. Morange, and A. Bertolotti. 2004. Targeting
752 expression of expanded polyglutamine proteins to the endoplasmic reticulum or mitochondria
753 prevents their aggregation. *Proc Natl Acad Sci U S A*. 101:9648-9653.
754 Rujano, M.A., F. Bosveld, F.A. Salomons, F. Dijk, M.A. van Waarde, J.J. van der Want, R.A. de Vos,
755 E.R. Brunt, O.C. Sibon, and H.H. Kampinga. 2006. Polarised asymmetric inheritance of
756 accumulated protein damage in higher eukaryotes. *PLoS Biol*. 4:e417.
757 Sackton, K.L., N. Dimova, X. Zeng, W. Tian, M. Zhang, T.B. Sackton, J. Meaders, K.L. Pfaff, F.
758 Sigoillot, H. Yu, X. Luo, and R.W. King. 2014. Synergistic blockade of mitotic exit by two
759 chemical inhibitors of the APC/C. *Nature*. 514:646-649.
760 Samanta, S., S. Yang, B. Debnath, D. Xue, Y. Kuang, K. Ramkumar, A.S. Lee, M. Ljungman, and N.
761 Neamati. 2021. The Hydroxyquinoline Analogue YUM70 Inhibits GRP78 to Induce ER Stress-
762 Mediated Apoptosis in Pancreatic Cancer. *Cancer Res*. 81:1883-1895.
763 Schlaitz, A.L., J. Thompson, C.C. Wong, J.R. Yates, 3rd, and R. Heald. 2013. REEP3/4 ensure
764 endoplasmic reticulum clearance from metaphase chromatin and proper nuclear envelope
765 architecture. *Dev Cell*. 26:315-323.
766 Sharma, R., M.M.D. Pramanik, B. Chandramouli, N. Rastogi, and N. Kumar. 2018. Understanding
767 organellar protein folding capacities and assessing their pharmacological modulation by
768 small molecules. *Eur J Cell Biol*. 97:114-125.
769 Shim, S.M., H.R. Choi, K.W. Sung, Y.J. Lee, S.T. Kim, D. Kim, S.R. Mun, J. Hwang, H. Cha-Molstad,
770 A. Ciechanover, B.Y. Kim, and Y.T. Kwon. 2018. The endoplasmic reticulum-residing
771 chaperone BiP is short-lived and metabolized through N-terminal arginylation. *Sci Signal*. 11.
772 Singhvi, A., and G. Garriga. 2009. Asymmetric divisions, aggresomes and apoptosis. *Trends Cell*
773 *Biol*. 19:1-7.
774 Tyedmers, J., A. Mogk, and B. Bukau. 2010. Cellular strategies for controlling protein aggregation.
775 *Nat Rev Mol Cell Biol*. 11:777-788.
776 Vincenz-Donnelly, L., H. Holthusen, R. Korner, E.C. Hansen, J. Presto, J. Johansson, R. Sawarkar,
777 F.U. Hartl, and M.S. Hipp. 2018. High capacity of the endoplasmic reticulum to prevent
778 secretion and aggregation of amyloidogenic proteins. *EMBO J*. 37:337-350.
779 Wang, C., J. Ding, Q. Wei, S. Du, X. Gong, and T.G. Chew. 2023. Mechanosensitive accumulation

780 of non-muscle myosin IIB during mitosis requires its translocation activity. *iScience*.
781 26:107773.
782 Watson, E.R., N.G. Brown, J.M. Peters, H. Stark, and B.A. Schulman. 2019. Posing the APC/C E3
783 Ubiquitin Ligase to Orchestrate Cell Division. *Trends Cell Biol*. 29:117-134.
784 Wirth, A.J., M. Platkov, and M. Gruebele. 2013. Temporal variation of a protein folding energy
785 landscape in the cell. *J Am Chem Soc*. 135:19215-19221.
786 Wiseman, R.L., J.S. Mesgarzadeh, and L.M. Hendershot. 2022. Reshaping endoplasmic reticulum
787 quality control through the unfolded protein response. *Mol Cell*. 82:1477-1491.
788 Woerner, A.C., F. Frottin, D. Hornburg, L.R. Feng, F. Meissner, M. Patra, J. Tatzelt, M. Mann, K.F.
789 Winklhofer, F.U. Hartl, and M.S. Hipp. 2016. Cytoplasmic protein aggregates interfere with
790 nucleocytoplasmic transport of protein and RNA. *Science*. 351:173-176.
791 Zhou, C., B.D. Slaughter, J.R. Unruh, F. Guo, Z. Yu, K. Mickey, A. Narkar, R.T. Ross, M. McClain,
792 and R. Li. 2014. Organelle-based aggregation and retention of damaged proteins in
793 asymmetrically dividing cells. *Cell*. 159:530-542.

794

Figure 1

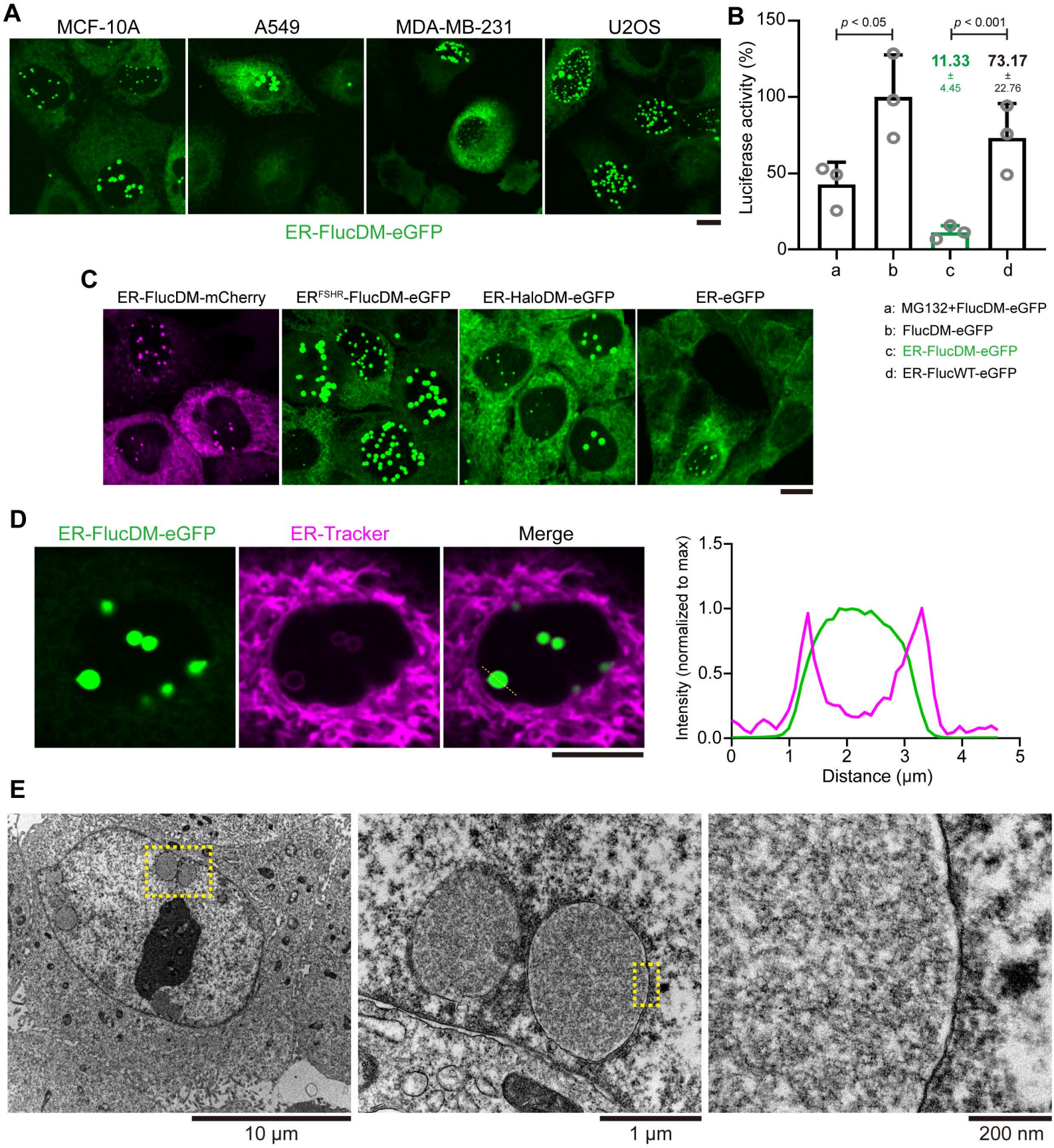
A
MCF-10A
A549
MDA-MB-231
U2OS
ER-FlucDM-eGFP
B
Luciferase activity (%)
150
100
50
0
p < 0.05
p < 0.001
11.33
±
4.45
73.17
±
22.76
a
b
c
d
a: MG132+FlucDM-eGFP
b: FlucDM-eGFP
c: ER-FlucDM-eGFP
d: ER-FlucWT-eGFP
C
ER-FlucDM-mCherry
ERFSHR-FlucDM-eGFP
ER-HaloDM-eGFP
ER-eGFP
D
ER-FlucDM-eGFP
ER-Tracker
Merge
Intensity (normalized to max)
1.5
1.0
0.5
0.0
0
1
2
3
4
5
Distance (μm)
E
10 μm
1 μm
200 nm

Figure 2

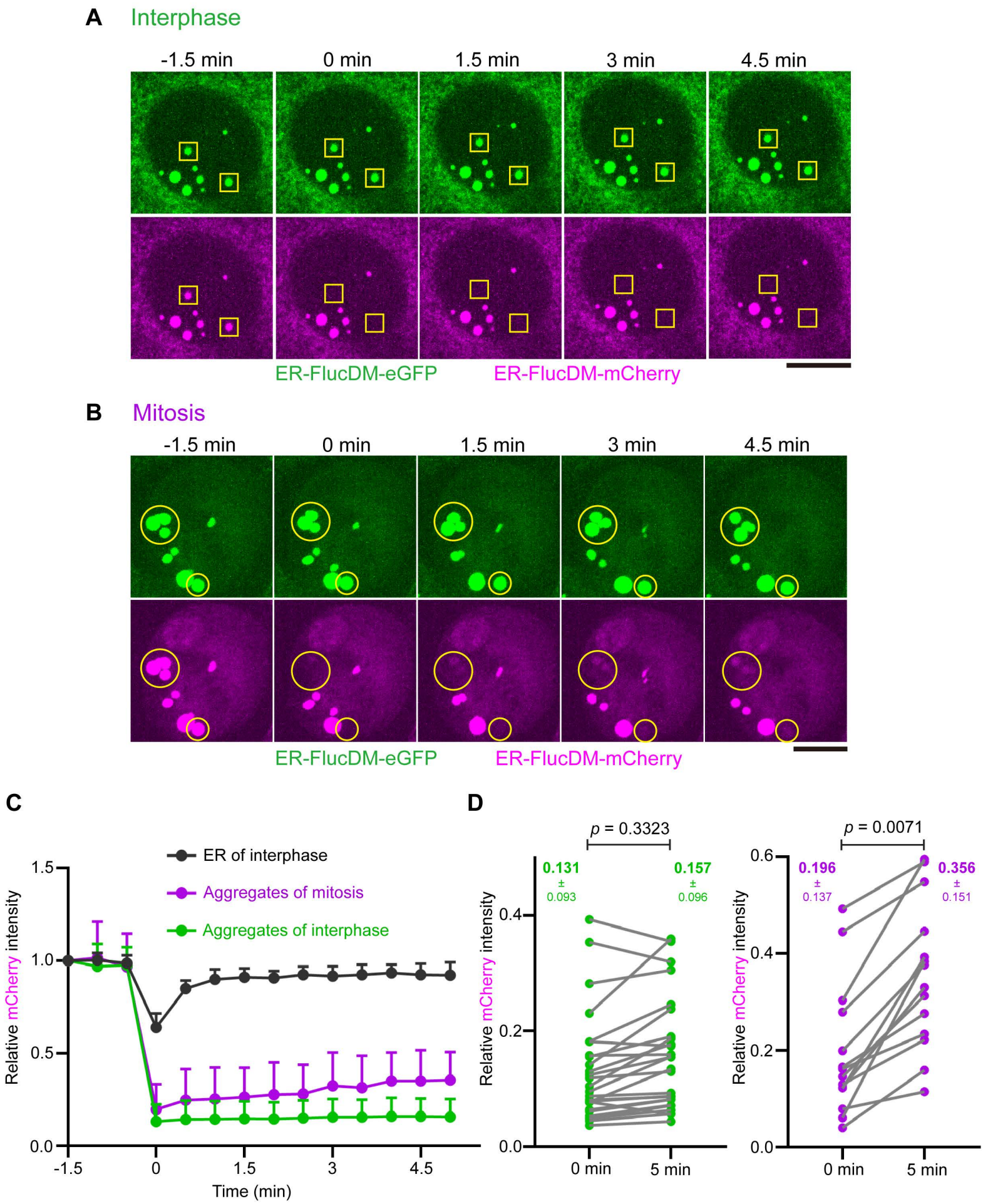
A
Interphase
-1.5 min
0 min
1.5 min
3 min
4.5 min
ER-FlucDM-eGFP
ER-FlucDM-mCherry
B
Mitosis
-1.5 min
0 min
1.5 min
3 min
4.5 min
ER-FlucDM-eGFP
ER-FlucDM-mCherry
C
ER of interphase
Aggregates of mitosis
Aggregates of interphase
Relative mCherry intensity
1.5
1.0
0.5
0.0
-1.5
0
1.5
3
4.5
Time (min)
D
p = 0.3323
0.131
±
0.093
0.157
±
0.096
Relative mCherry intensity
0.4
0.2
0.0
0 min
5 min
p = 0.0071
0.196
±
0.137
0.356
±
0.151
Relative mCherry intensity
0.6
0.4
0.2
0.0
0 min
5 min

Figure 3

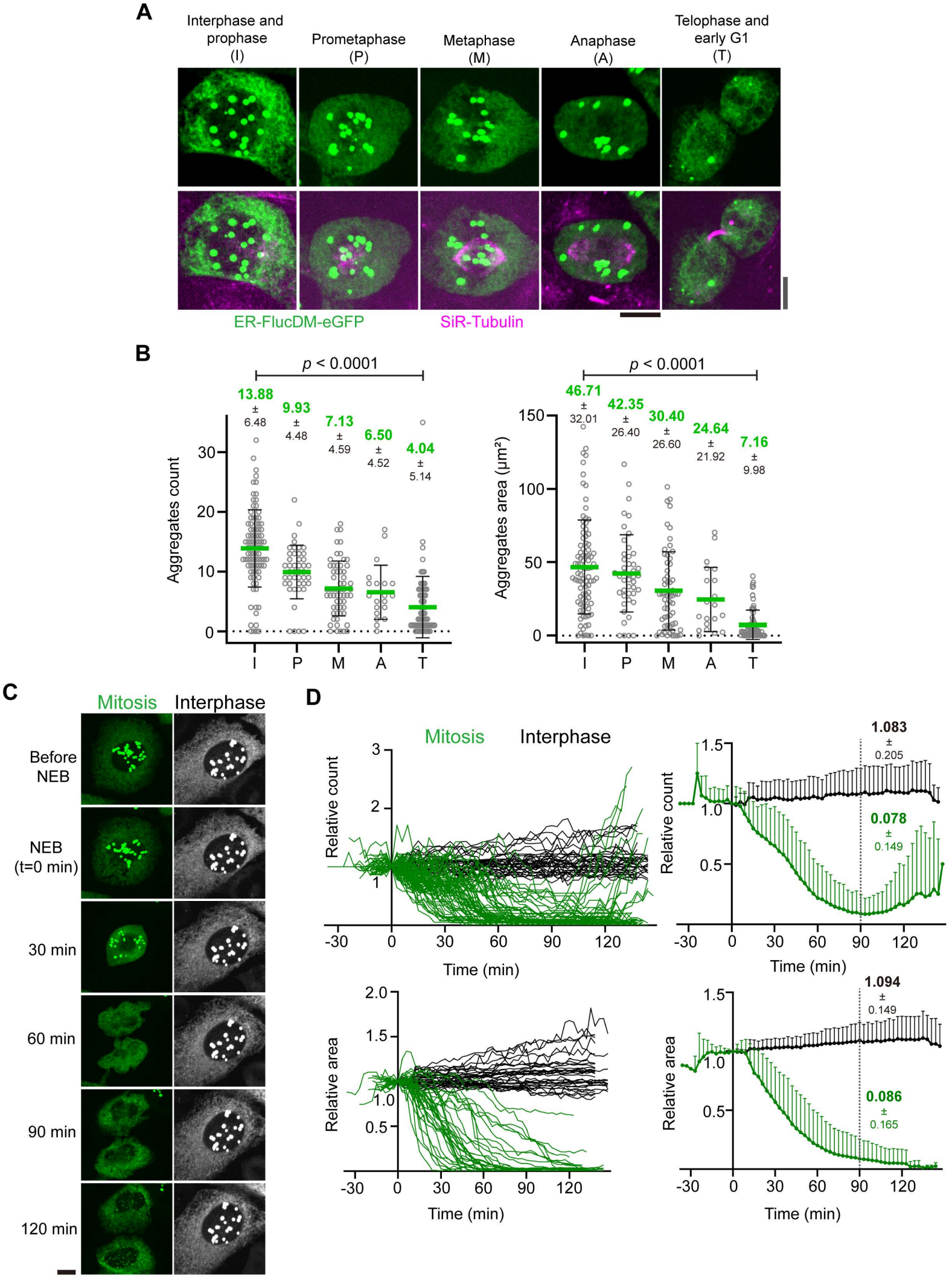
A
Interphase and prophase (I)
Prometaphase (P)
Metaphase (M)
Anaphase (A)
Telophase and early G1 (T)
ER-FlucDM-eGFP
SiR-Tubulin
B
p < 0.0001
Aggregates count
13.88 ± 6.48
9.93 ± 4.48
7.13 ± 4.59
6.50 ± 4.52
4.04 ± 5.14
I P M A T
p < 0.0001
Aggregates area (µm²)
46.71 ± 32.01
42.35 ± 26.40
30.40 ± 26.60
24.64 ± 21.92
7.16 ± 9.98
I P M A T
C
Mitosis
Interphase
Before NEB
NEB (t=0 min)
30 min
60 min
90 min
120 min
D
Mitosis
Interphase
Relative count
Time (min)
1.083 ± 0.205
0.078 ± 0.149
Relative area
1.094 ± 0.149
0.086 ± 0.165

Figure 4

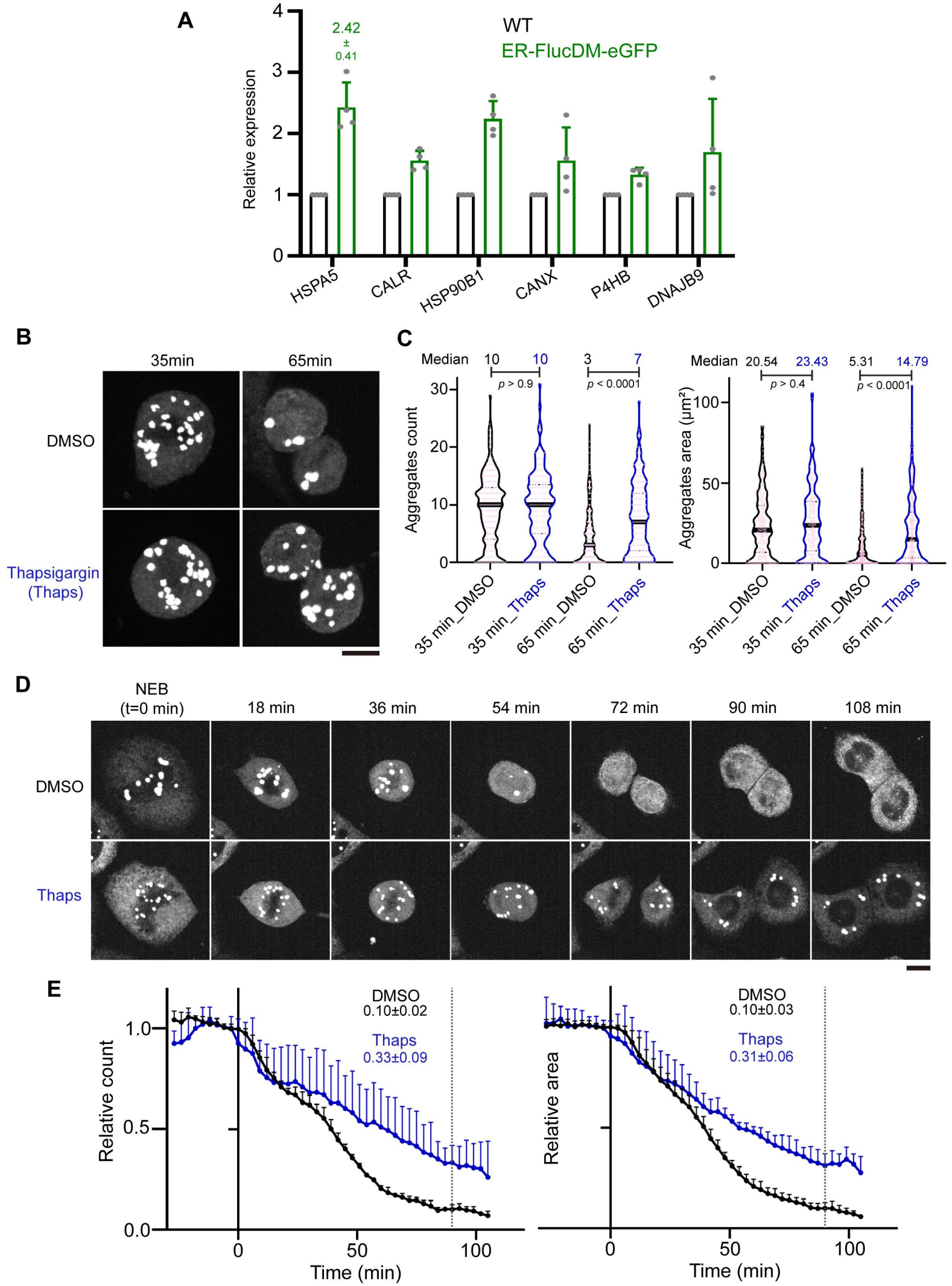
A
WT
ER-FlucDM-eGFP
2.42
±
0.41
Relative expression
HSPA5
CALR
HSP90B1
CANX
P4HB
DNAJB9
B
35min
65min
DMSO
Thapsigargin
(Thaps)
C
Median 10 10 3 7
p > 0.9
p < 0.0001
Aggregates count
Median 20.54 23.43 5.31 14.79
p > 0.4
p < 0.0001
Aggregates area (µm²)
35 min_DMSO
35 min_Thaps
65 min_DMSO
65 min_Thaps
D
NEB
(t=0 min)
18 min
36 min
54 min
72 min
90 min
108 min
DMSO
Thaps
E
DMSO
0.10±0.02
Thaps
0.33±0.09
Relative count
DMSO
0.10±0.03
Thaps
0.31±0.06
Relative area
Time (min)

Figure 5

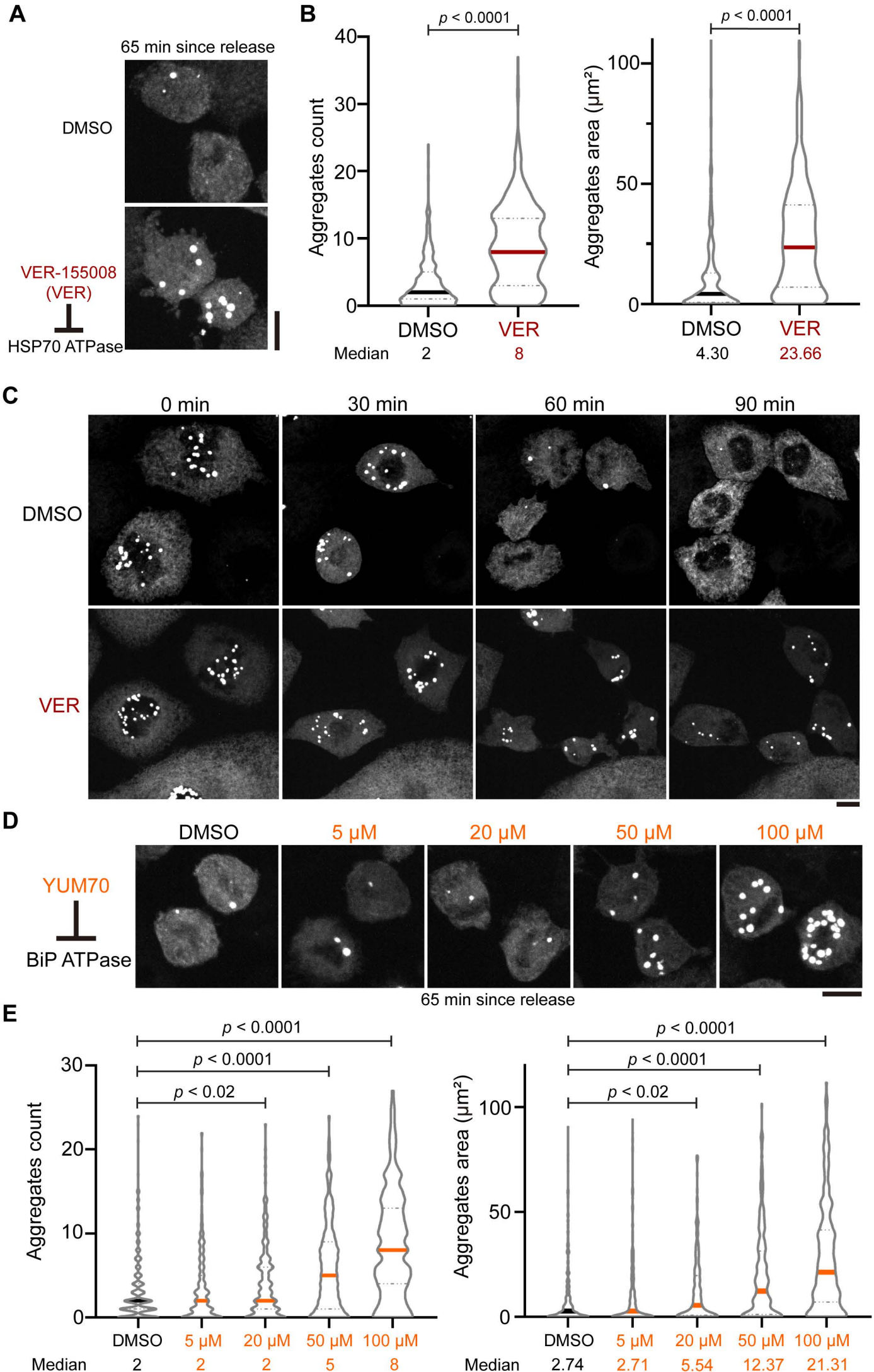
A
65 min since release
DMSO
VER-155008
(VER)
HSP70 ATPase
B
p < 0.0001
Aggregates count
DMSO
VER
Median
2
8
p < 0.0001
Aggregates area (µm²)
DMSO
VER
4.30
23.66
C
0 min
30 min
60 min
90 min
DMSO
VER
D
DMSO
5 µM
20 µM
50 µM
100 µM
YUM70
BiP ATPase
65 min since release
E
p < 0.0001
p < 0.0001
p < 0.02
Aggregates count
DMSO
5 µM
20 µM
50 µM
100 µM
Median
2
2
2
5
8
p < 0.0001
p < 0.0001
p < 0.02
Aggregates area (µm²)
DMSO
5 µM
20 µM
50 µM
100 µM
Median
2.74
2.71
5.54
12.37
21.31

Figure 6

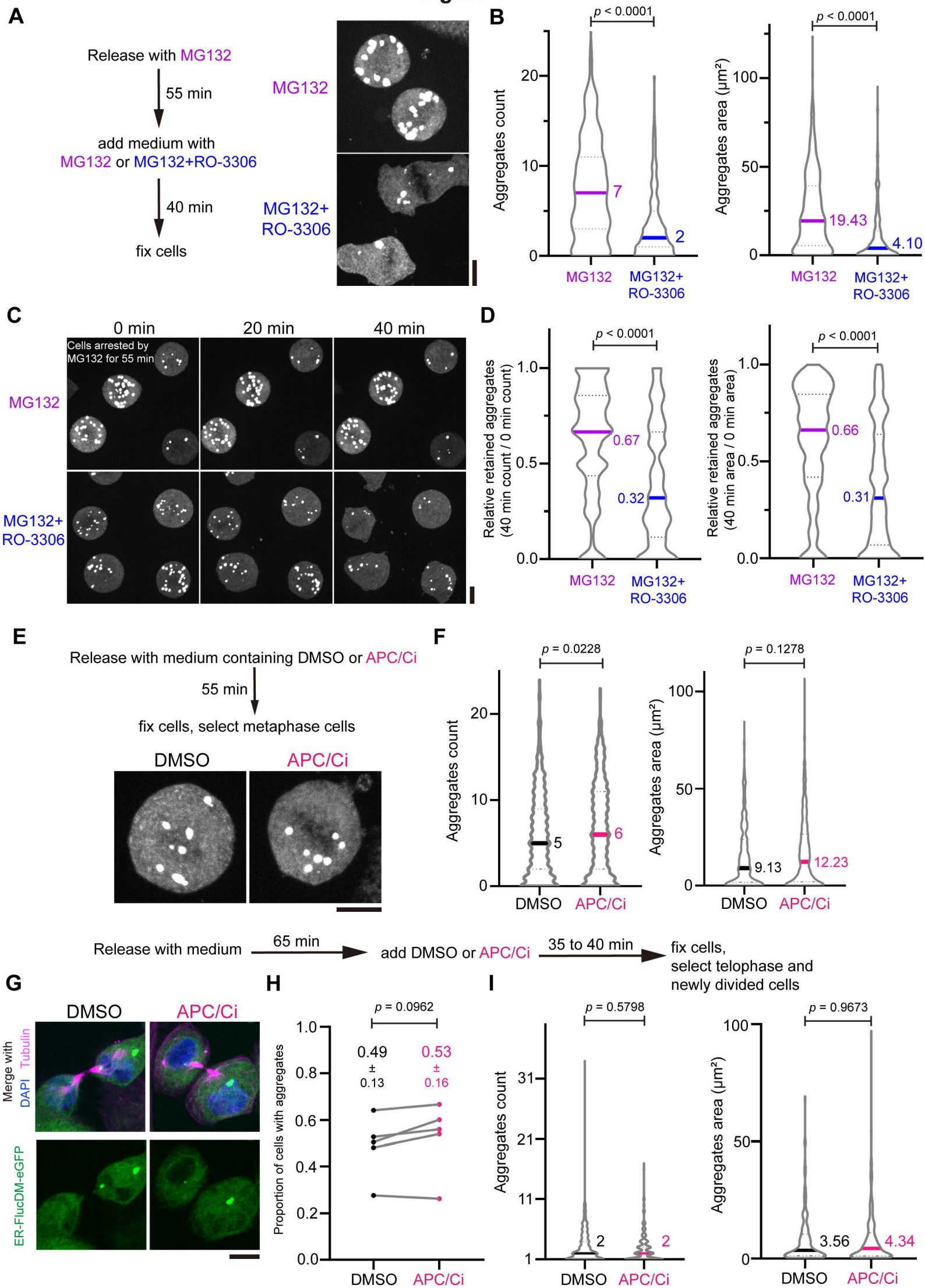
A
Release with MG132
55 min
add medium with
MG132 or MG132+RO-3306
40 min
fix cells
MG132
MG132+
RO-3306
B
p < 0.0001
Aggregates count
7
2
MG132
MG132+
RO-3306
p < 0.0001
Aggregates area (μm²)
19.43
4.10
MG132
MG132+
RO-3306
C
0 min
20 min
40 min
Cells arrested by
MG132 for 55 min
MG132
MG132+
RO-3306
D
p < 0.0001
Relative retained aggregates
(40 min count / 0 min count)
0.67
0.32
MG132
MG132+
RO-3306
p < 0.0001
Relative retained aggregates
(40 min area / 0 min area)
0.66
0.31
MG132
MG132+
RO-3306
E
Release with medium containing DMSO or APC/Ci
55 min
fix cells, select metaphase cells
DMSO
APC/Ci
F
p = 0.0228
Aggregates count
5
6
DMSO
APC/Ci
p = 0.1278
Aggregates area (μm²)
9.13
12.23
DMSO
APC/Ci
Release with medium
65 min
add DMSO or APC/Ci
35 to 40 min
fix cells,
select telophase and
newly divided cells
G
DMSO
APC/Ci
Merge with
DAPI Tubulin
ER-FlucDM-eGFP
H
p = 0.0962
Proportion of cells with aggregates
0.49
±
0.13
0.53
±
0.16
DMSO
APC/Ci
I
p = 0.5798
Aggregates count
2
2
DMSO
APC/Ci
p = 0.9673
Aggregates area (μm²)
3.56
4.34
DMSO
APC/Ci

Figure S1

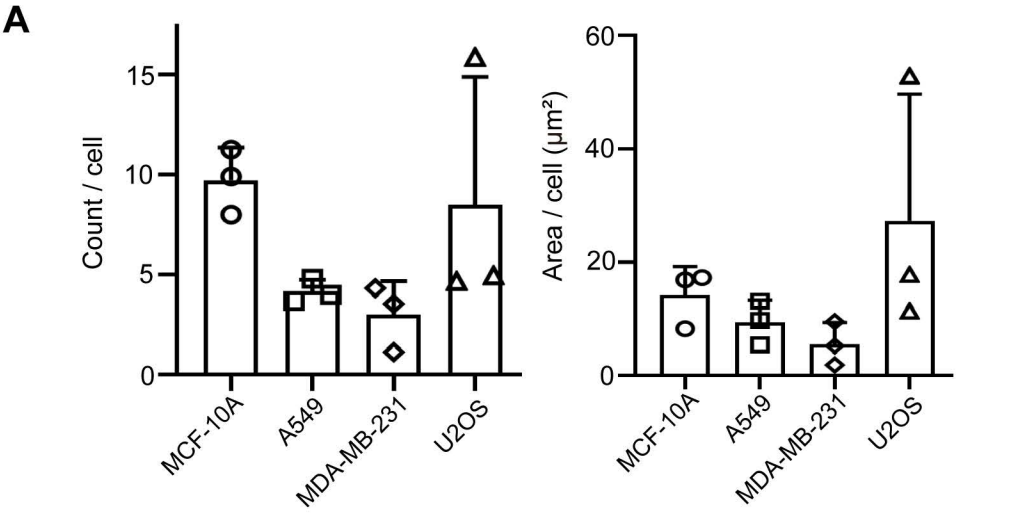
A
Count / cell
15
10
5
0
MCF-10A
A549
MDA-MB-231
U2OS
Area / cell (μm²)
60
40
20
0
MCF-10A
A549
MDA-MB-231
U2OS

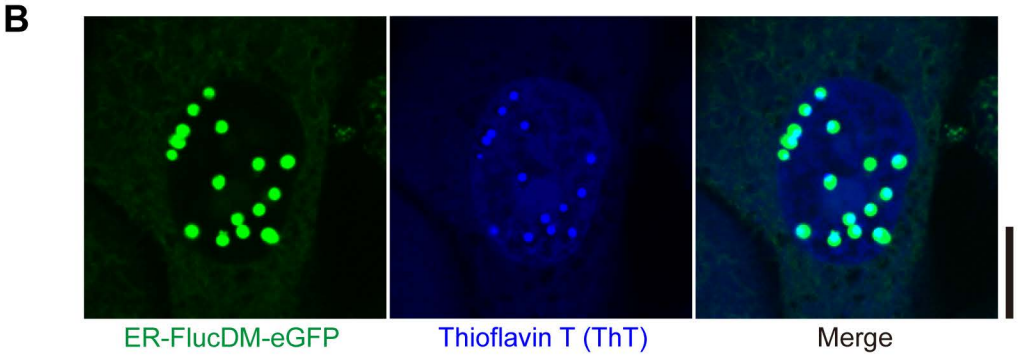
B
ER-FlucDM-eGFP
Thioflavin T (ThT)
Merge

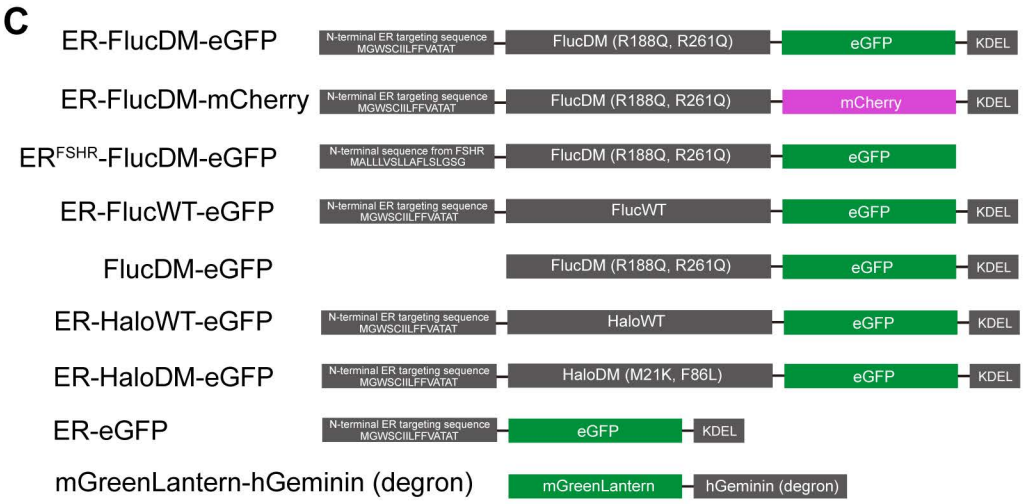
C
ER-FlucDM-eGFP
N-terminal ER targeting sequence MGWSCIILFFVATAT
FlucDM (R188Q, R261Q)
eGFP
KDEL
ER-FlucDM-mCherry
mCherry
ERFSHR-FlucDM-eGFP
N-terminal sequence from FSHR MALLLVSLLAFLSLGSG
ER-FlucWT-eGFP
FlucWT
FlucDM-eGFP
ER-HaloWT-eGFP
HaloWT
ER-HaloDM-eGFP
HaloDM (M21K, F86L)
ER-eGFP
mGreenLantern-hGeminin (degron)
mGreenLantern
hGeminin (degron)

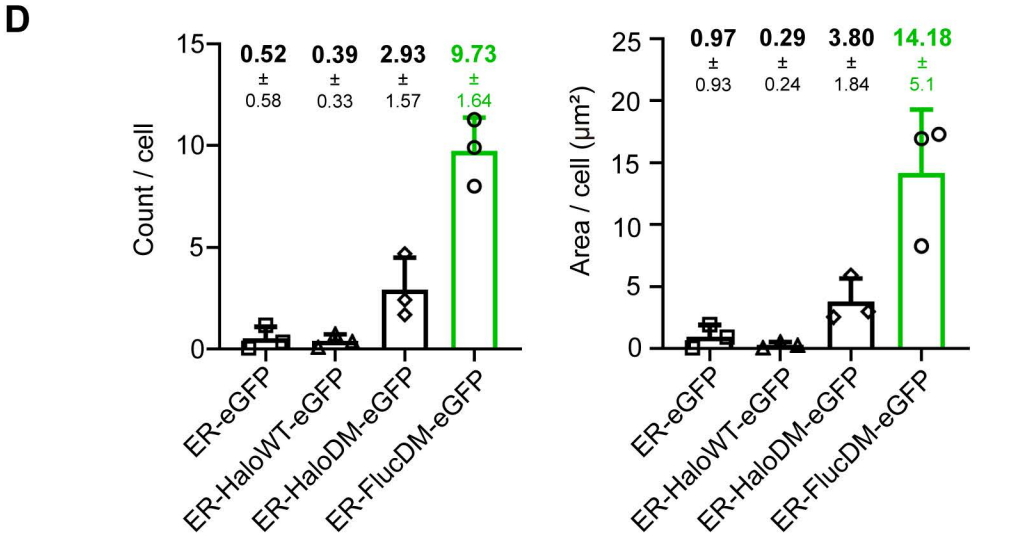
D
Count / cell
15
10
5
0
0.52 ± 0.58
0.39 ± 0.33
2.93 ± 1.57
9.73 ± 1.64
ER-eGFP
ER-HaloWT-eGFP
ER-HaloDM-eGFP
ER-FlucDM-eGFP
Area / cell (μm²)
25
20
15
10
5
0
0.97 ± 0.93
0.29 ± 0.24
3.80 ± 1.84
14.18 ± 5.1
ER-eGFP
ER-HaloWT-eGFP
ER-HaloDM-eGFP
ER-FlucDM-eGFP

Figure S2

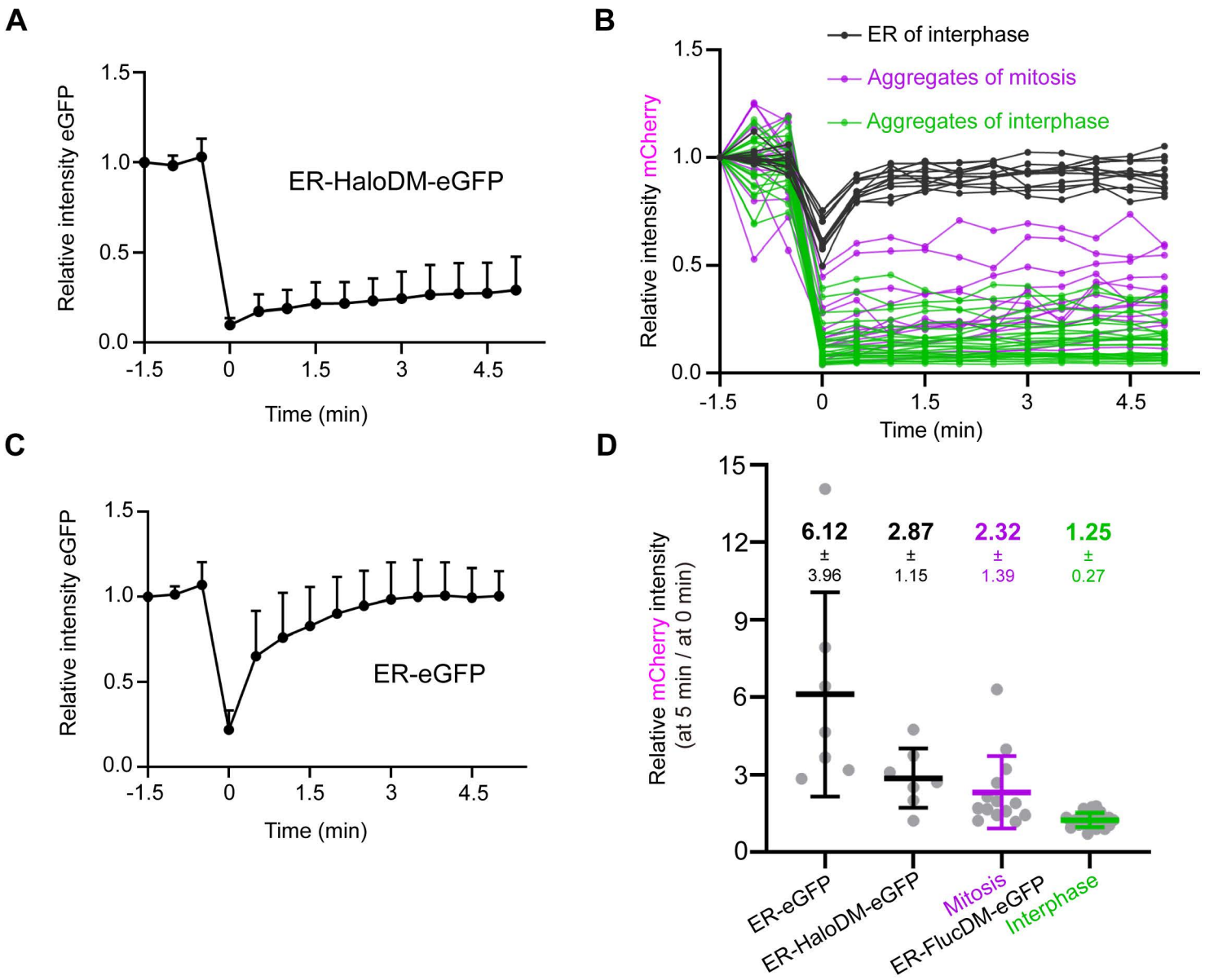
A
Relative intensity eGFP
ER-HaloDM-eGFP
Time (min)
B
ER of interphase
Aggregates of mitosis
Aggregates of interphase
Relative intensity mCherry
Time (min)
C
Relative intensity eGFP
ER-eGFP
Time (min)
D
Relative mCherry intensity
(at 5 min / at 0 min)
6.12 ± 3.96
2.87 ± 1.15
2.32 ± 1.39
1.25 ± 0.27
ER-eGFP
ER-HaloDM-eGFP
Mitosis
ER-FlucDM-eGFP
Interphase

Figure S3

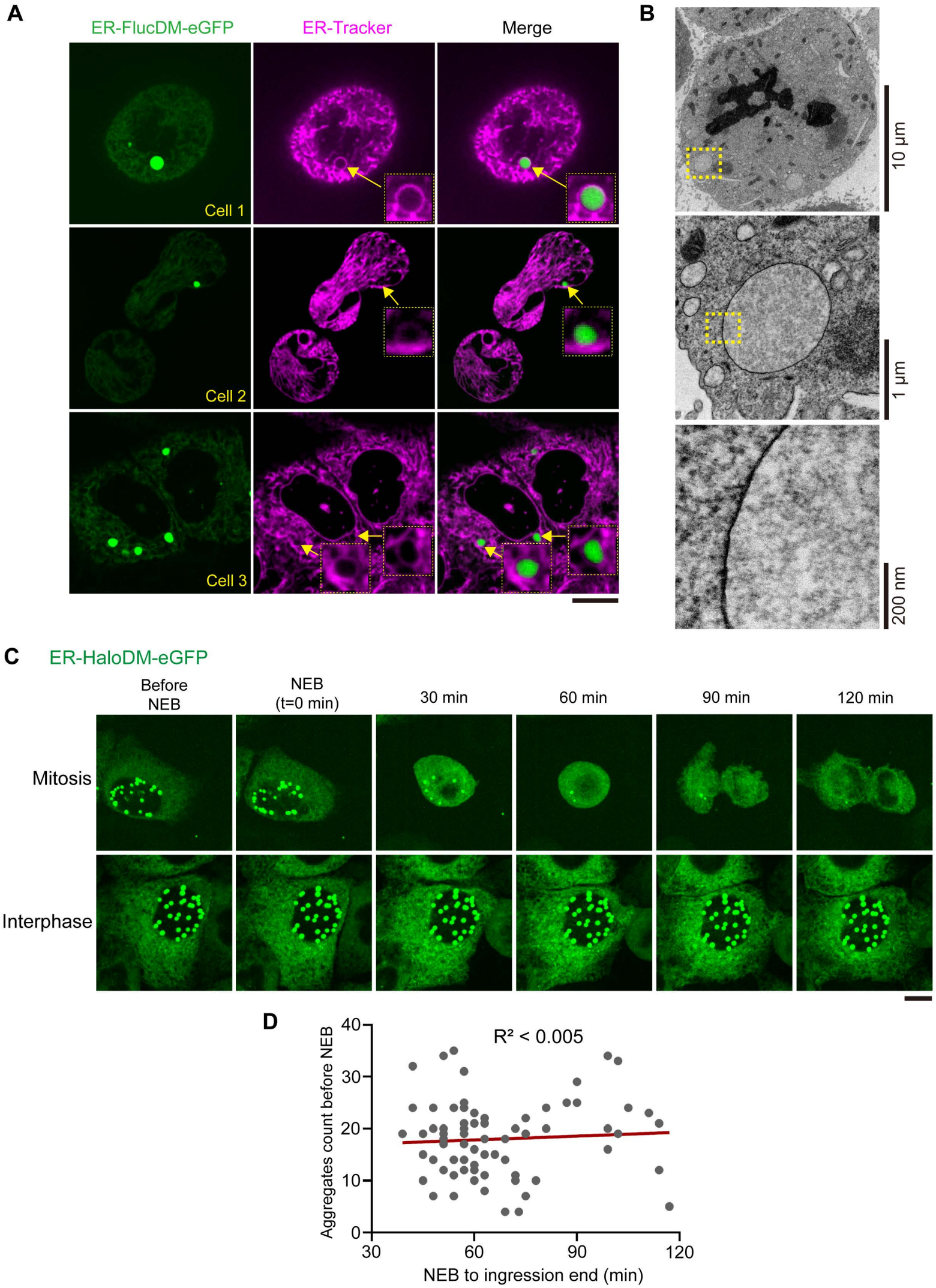
A
ER-FlucDM-eGFP
ER-Tracker
Merge
Cell 1
Cell 2
Cell 3
B
10 µm
1 µm
200 nm
C
ER-HaloDM-eGFP
Before NEB
NEB (t=0 min)
30 min
60 min
90 min
120 min
Mitosis
Interphase
D
R² < 0.005
Aggregates count before NEB
NEB to ingression end (min)
0
10
20
30
40
30
60
90
120

Figure S4

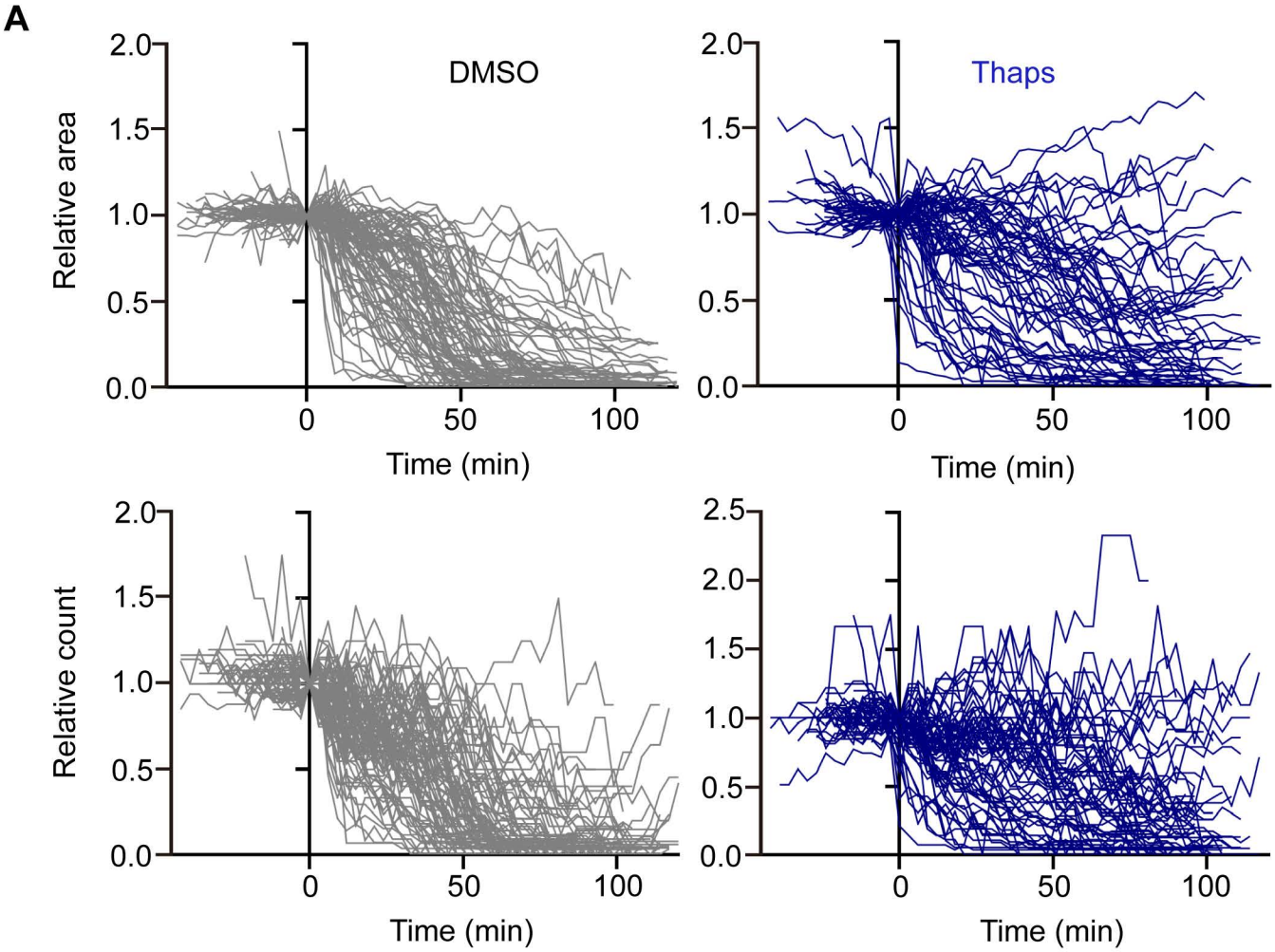
A
DMSO
Thaps
Relative area
Relative count
Time (min)
2.0
1.5
1.0
0.5
0.0
2.5
0
50
100

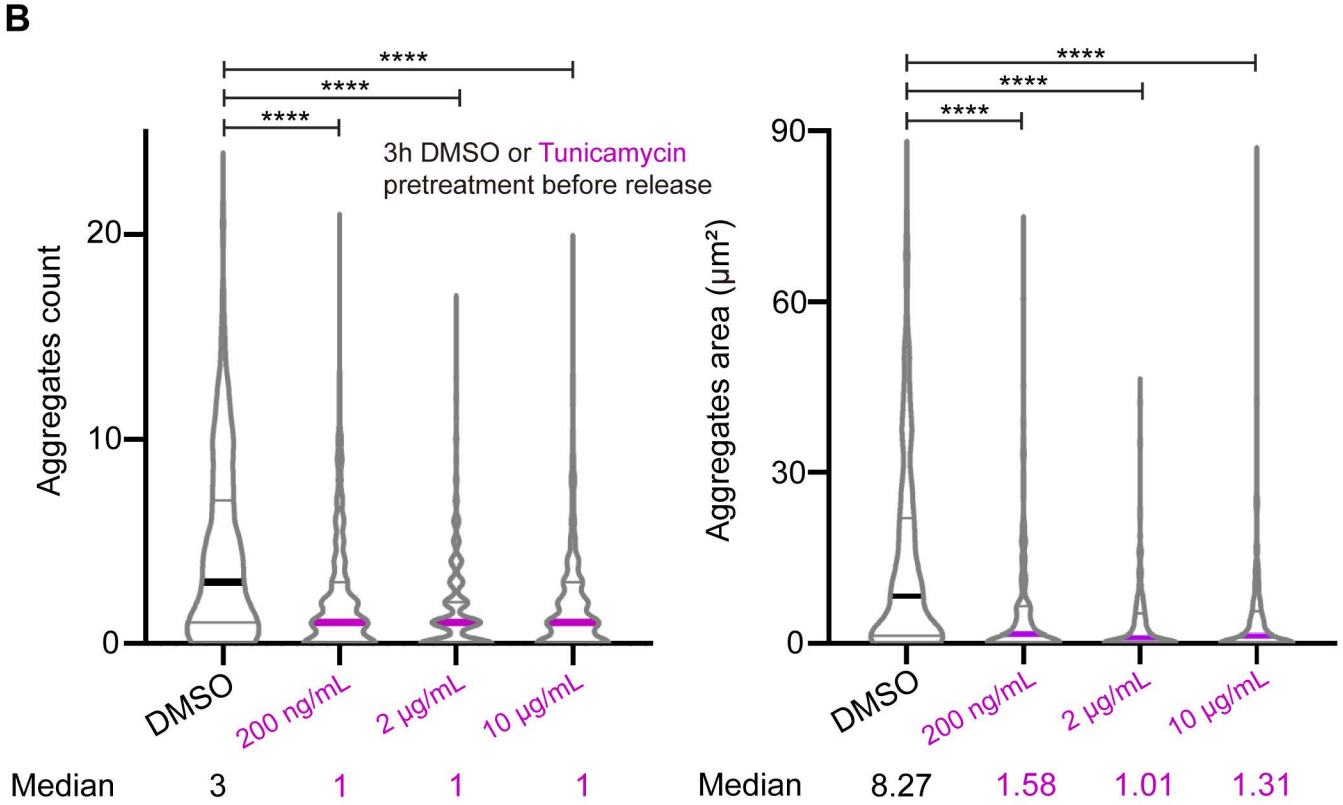
B
****
3h DMSO or Tunicamycin
pretreatment before release
Aggregates count
Aggregates area (µm²)
DMSO
200 ng/mL
2 µg/mL
10 µg/mL
Median 3 1 1 1
Median 8.27 1.58 1.01 1.31

Figure S5

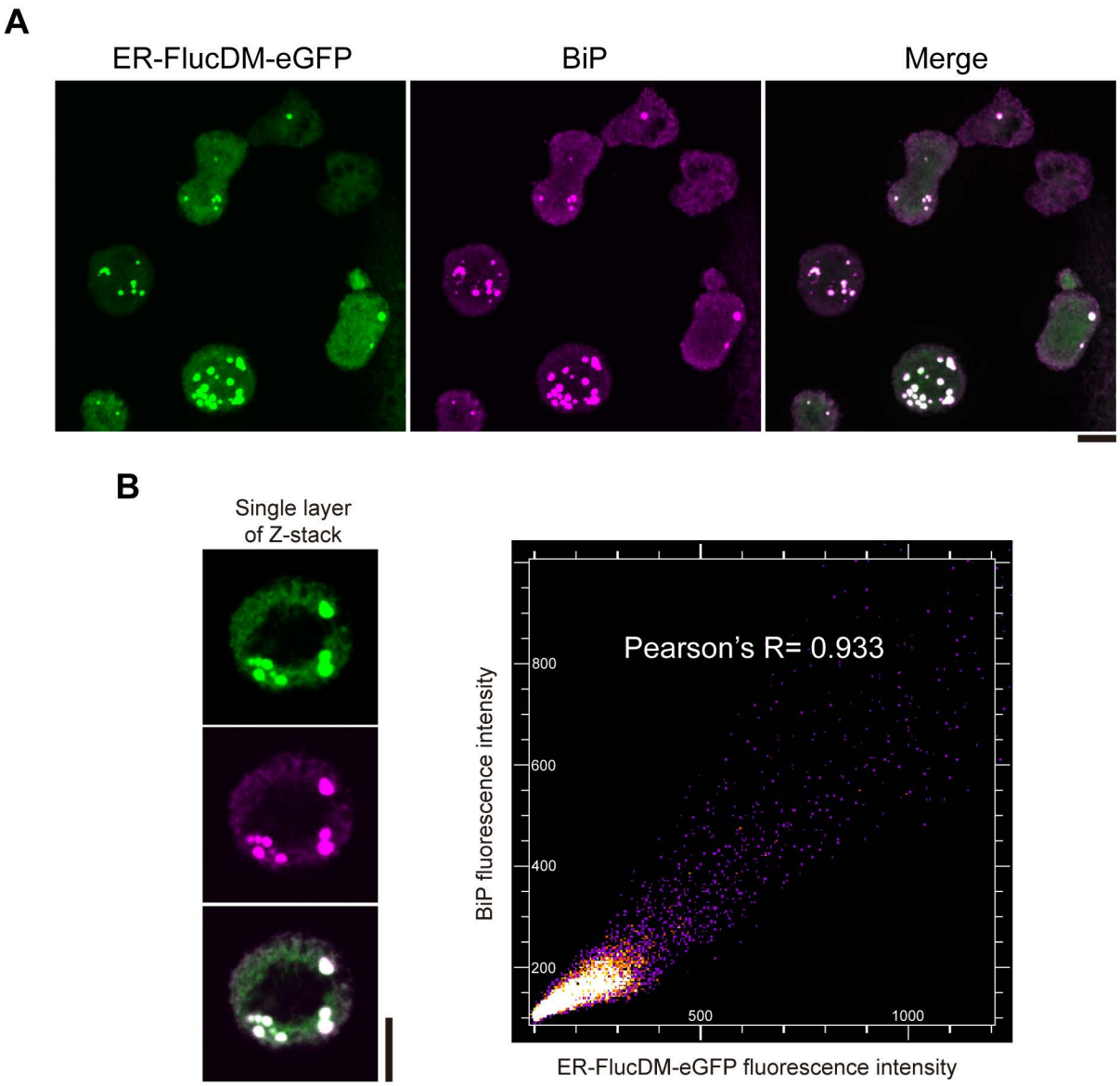
A
ER-FlucDM-eGFP
BiP
Merge
B
Single layer
of Z-stack
Pearson's R= 0.933
BiP fluorescence intensity
800
600
400
200
500
1000
ER-FlucDM-eGFP fluorescence intensity

Figure S6

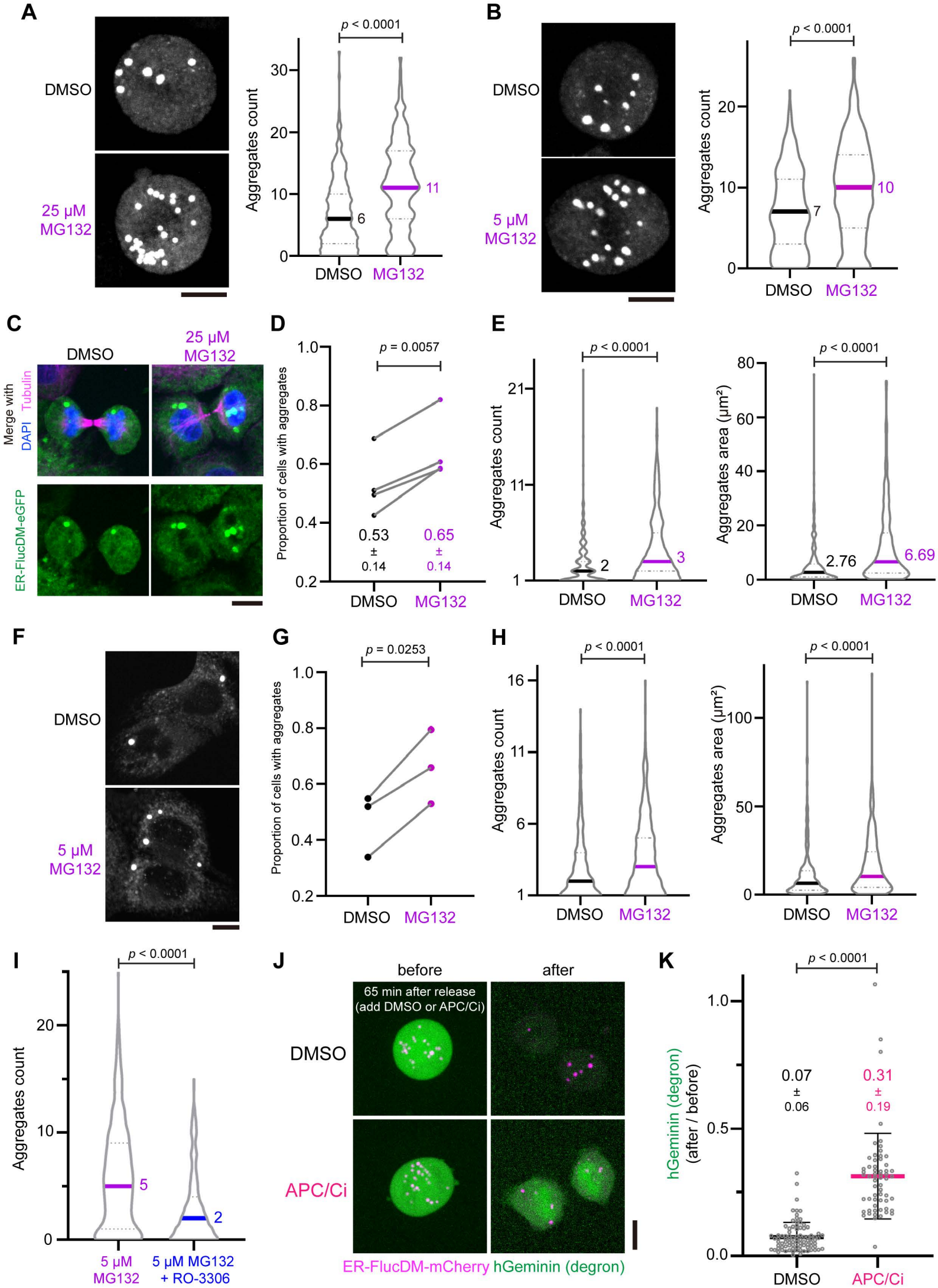
A
DMSO
25 μM MG132
p < 0.0001
Aggregates count
6
11
DMSO
MG132
B
DMSO
5 μM MG132
p < 0.0001
Aggregates count
7
10
DMSO
MG132
C
DMSO
25 μM MG132
Merge with DAPI Tubulin
ER-FlucDM-eGFP
D
p = 0.0057
Proportion of cells with aggregates
0.53 ± 0.14
0.65 ± 0.14
DMSO
MG132
E
p < 0.0001
Aggregates count
2
3
p < 0.0001
Aggregates area (μm²)
2.76
6.69
DMSO
MG132
F
DMSO
5 μM MG132
G
p = 0.0253
Proportion of cells with aggregates
DMSO
MG132
H
p < 0.0001
Aggregates count
p < 0.0001
Aggregates area (μm²)
DMSO
MG132
I
p < 0.0001
Aggregates count
5
2
5 μM MG132
5 μM MG132 + RO-3306
J
before
after
65 min after release (add DMSO or APC/Ci)
DMSO
APC/Ci
ER-FlucDM-mCherry
hGeminin (degron)
K
p < 0.0001
hGeminin (degron) (after / before)
0.07 ± 0.06
0.31 ± 0.19
DMSO
APC/Ci